Geological Quarterly, 2023, 67: 43
DOI: http://dx.doi.org/10.7306/gq.1713

The genesis of base and precious metals-bearing epithermal veins in the Gharehchay-Kurmolla area, south of Tikmehdash, NW Iran

Zahra HASSANI SOUGHI[1, *], Ali Asghar CALAGARI[1] and Ghahraman SOHRABI[2]

[1] University of Tabriz, Faculty of Natural Sciences, Department of Earth Sciences, Tabriz, Iran

[2] University of Mohaghegh Ardabili, Faculty of Basic Sciences, Department of Geology, Ardabil, Iran

Soughi, Z.H., Calagari, A.A., Sohrabi, G., 2023. The genesis of base and precious metals-bearing epithermal veins in the Gharehchay-Kurmolla area, south of Tikmehdash, NW Iran. Geological Quarterly, 2023, 67: 43; http://dx.doi.org/10.7306/gq.1713

Associate Editor: Stanisław Z. Mikulski

The Gharehchay-Kurmolla (Gh-Ku) base and precious metals occurrence is located in ~2 km south of Tikmehdash, 75 km south-east of Tabriz, and is a part of Bostanabad-Miyaneh gold-bearing district in the West Alborz-Azarbaidjan structural zone. Mineralization in the study area occurs in quartz veins and veinlets hosted by the Eocene volcanic-pyroclastic units as well as granite. Recognizable alteration zones around the quartz veins and veinlets include silicic, phyllic, intermediate argillic, and propylitic types. The mineralization was developed during three conspicuous stages. In stage 1, minerals such as quartz, pyrite, and chalcopyrite with slight amounts of gold were formed. During stage 2, minerals such as quartz, galena, sphalerite, and gold together with pyrite and chalcopyrite were developed. Stage 3 was concurrent with deposition of quartz accompanied by Mn-oxides and hydroxides (pyrolusite and psilomelane). The major gangue minerals are quartz, adularia, sericite, epidote, chlorite and calcite. Micro-thermometric investigations on primary 2-phase (LV) fluid inclusions in quartz crystals showed that the hydrothermal fluids responsible for mineralization had temperatures and salinities ranging from 215 to 325 C and from 2.6 to 10.4 wt.% NaCl eq., respectively. The oxygen isotopic composition of the fluid (+9.7 to +12.5‰) suggests that the ore-forming solutions had a largely magmatic component. The sulphur isotopic composition of the fluid (–1.5 to –3.4‰) is also indicative of magmatic origin. On the basis of data obtained from micro-thermometric and stable isotope analyses, boiling along with mixing were two important mechanisms involved in the precipitation of ore and gangue minerals in the study area. The geological and geochemical characteristics of the Gh-Ku area indicate that mineralization in this area is of epithermal type with a low-sulphidation style.

Key words: Tikmehdash, Au-bearing quartz veins, low-sulphidation, epithermal, micro-thermometric analysis, stable isotopes.

INTRODUCTION

Epithermal deposits are recognized as valuable base (Cu, Pb, and Zn) and precious (Au and Ag) metal resources (Simmons et al., 2005). These deposits are commonly formed at depths from <1 to 1.5 km in low to intermediate temperature (50 to 300 C) conditions by relatively low-salinity (5 to 15 wt.%) fluids (Cooke and Simmons, 2000; Simmons et al., 2005; Pirajno, 2009). These epithermal deposits are categorized into three styles: (1) low-sulphidation (LS), (2) intermediate-sulphidation (IS), and (3) high-sulphidation (HS) (White and Hedenquist, 1990; Hedenquist et al., 2000; Cooke and Simmons, 2000; Sillitoe and Hedenquist, 2003; Einaudi et al., 2003; Simmons et al., 2005).

Iran, situated in the middle part of the gigantic Alpine-Himalayan Belt, was always a suitable location for the development of epithermal base and precious metal deposits (Richards et al., 2006). In recent years, extensive research has taken place concerning the genesis and evolution of hydrothermal fluids associated with epithermal base and precious metal deposits in north-west Iran (Heidari et al., 2015; Mehrabi et al., 2016; Zamanian et al., 2019; Kouhestani et al., 2019a, b, 2020; Miranvari et al., 2020; Ferdowsi et al., 2021; Ebrahimi et al., 2021; Ghasemi Siani et al., 2022).

The Gharehchay-Kurmolla (Gh-Ku) base and precious metals occurrence is located ~2 km south of Tikmehdash, 75 km south-east of Tabriz, east-Azarbaidjan province, NW Iran. This mineral prospect is a part of the Bostanabad-Miyaneh gold-bearing district in the West Alborz-Azarbaidjan structural zone (Nabavi, 1976; Fig. 1). Eocene volcanism in this district produced a succession of volcanic-pyroclastic rocks which were intruded by Oligocene plutonic rocks. The hydrothermal fluids released

* Corresponding author, e-mail: z.hassanisoughi@tabrizu.ac.ir
Received: June 10, 2023; accepted: August 9, 2023; first published online: January 1, 2024

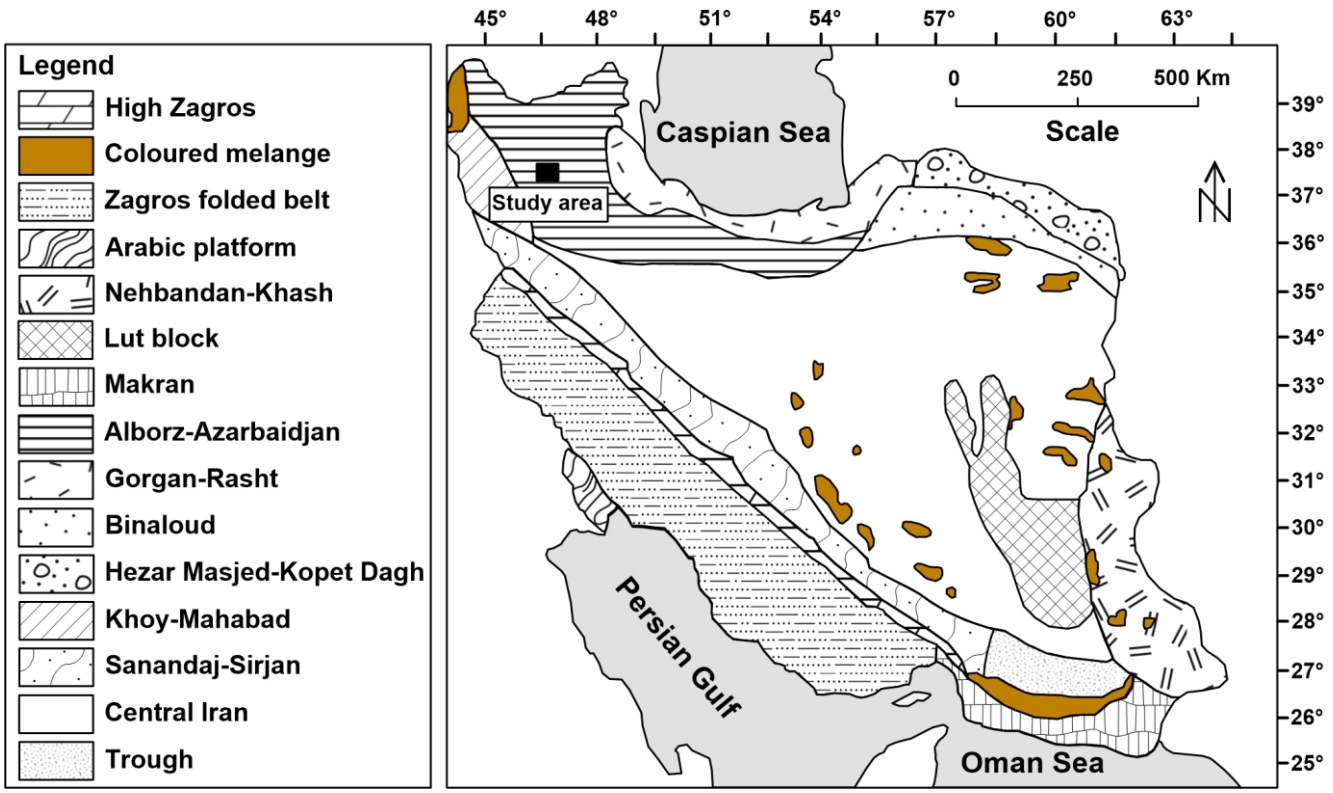

Fig. 1. An index map showing the major geological-structural divisions of Iran (Nabavi, 1976)

The location of the study area is marked (filled square)

from these intrusives was a source of alteration and mineralization in this district (Maghsoudi et al., 2005). Except for preliminary studies by Hassani Soughi et al. (2021), no other comprehensive scientific research on these hydrothermal fluids has been done so far. We have investigated the alteration and mineralization processes and analysed certain physico-chemical conditions controlling the ore deposition via constraints based on fluid inclusion and stable isotope data from the study area. The results of this research can contribute to better understanding and exploration of similar deposits in this district.

GEOLOGICAL SETTING

The Bostanabad-Miyaneh gold-bearing district starts from east of Miyaneh and extends to the west of Bostanabad, and is bounded to the north by the Bozghoosh mountain range. A large part of the district is covered by Paleogene volcanic rocks. Extensive volcanism took place in this district as the result of an extensional phase of the Laramide orogeny (Maghsoudi et al., 2005). The widespread volcanic rocks include lavas of latite, trachyandesite, basalt, dacite, and rhyolite composition with associated pyroclastic deposits. Oligocene intrusive rocks in the district occur as stocks, laccoliths, dikes, and sills intruding the Eocene volcanic rocks. In general, all the igneous rocks (both extrusive and intrusive) in the district were folded during the Alpine (Pyrenean) Orogeny. The volcanic activities continued until the Miocene as shown by the presence of volcanic rocks (lavas and pyroclastics) together with shallow marine deposits. Pliocene strata (gypsiferous marl and conglomerate) unconformably overlie the Miocene sequence (Maghsoudi et al., 2005).

According to the geological map of the Bostanabad quadrangle (1:100,000) (Behrouzi et al., 1997) and the map (1:5000) prepared by the authors (Fig. 2), the lithological units in the Gh-Ku area consist of Eocene volcanic lavas and pyroclastics with Oligocene intrusive bodies (e.g., granite). The oldest units cropped out in the area belong to Eocene (E^t, E^v, and E^{tv}) and these host the ore-bearing veins and veinlets. Unit E^{tv} consists of tuffs, some sandy, and green andesitic lavas (Fig. 3A) and crops out mainly near the granite with which it has a sharp contact. Following the intrusion of the granite, the accompanying hydrothermal fluids brought about alteration and mineralization in the E^{tv} unit. Unit E^v (younger than E^{tv}) is pale in colour and comprises porphyrytic andesite and andesitic basalt (Fig. 3A). It has suffered intense alteration in places, where in contact with granite, and is dark purple. Unit E^t consists of tuff breccias and pyroclastic rocks (Fig. 3B). In general, the Eocene lavas have porphyritic texture with microlithic matrix. The Oligocene intrusive bodies include the T^{gr} unit. This unit (granite) hosts part of the mineralization in the area (Fig. 3C). The principal structural features in the Gh-Ku area include a group of fault systems trending NW–SE and NE–SW. Those faults striking NW–SE have almost similar trends to the well-known Tabriz Fault and have a dextral strike-slip component, while the faults striking NE–SW have a sinistral strike-slip component. Generally, these faults had a controlling role on the ore-bearing quartz veins and veinlets in the study area.

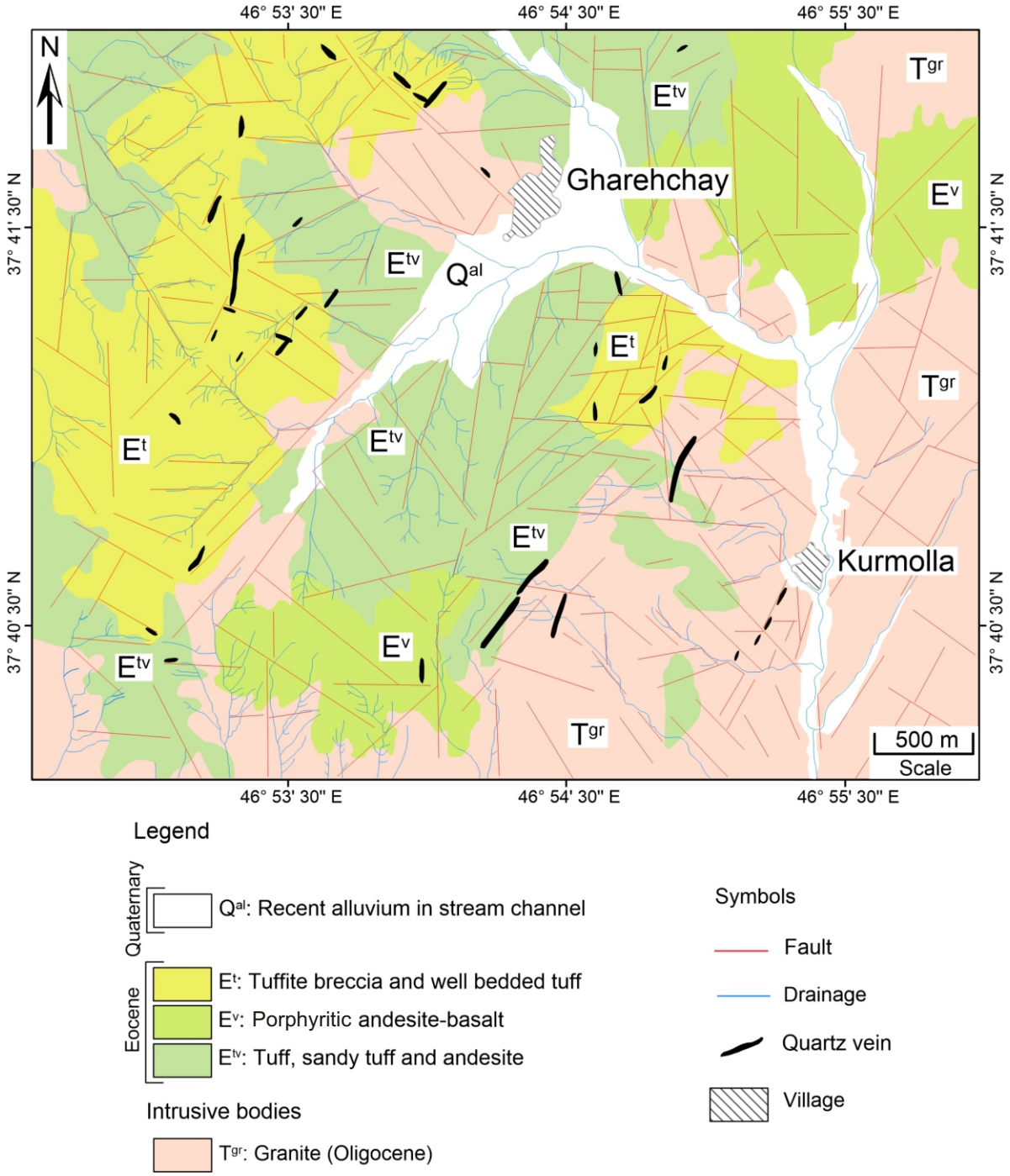

Fig. 2. Geologic map of the study area on which the locations and trends of the ore-bearing quartz veins are shown (modified after Behrouzi et al., 1997)

METHODS

Investigations took place both in the field and laboratory. During the fieldwork, a geological map (1:5000) was prepared and the ore-bearing veins and the associated host rocks were identified. Approximately 100 representative surface and subsurface samples were collected from the ore zones and host rocks. Laboratory work include preparation and examination of 15 thin and 30 polished thin-sections. Further mineralogical studies were made by scanning electron microscopy (SEM). This work was carried out in the Central Laboratories of the University of Tabriz using a *Tescan MIRA3 FEG-SEM* at 0.56 nA and accelerating voltage 15 kV. Ten doubly polished wafers were prepared for fluid inclusion studies. Micro-thermometric analysis took place using a *Linkam THMSG600* stage. Calibration of the measurements was ensured via the melting point of a sodium nitrate standard (+306.8°C) during heating (with an accuracy of ±0.6°C) and by the freezing point of a carbon tetrachloride standard (–22.99°C) during cooling (with an accuracy

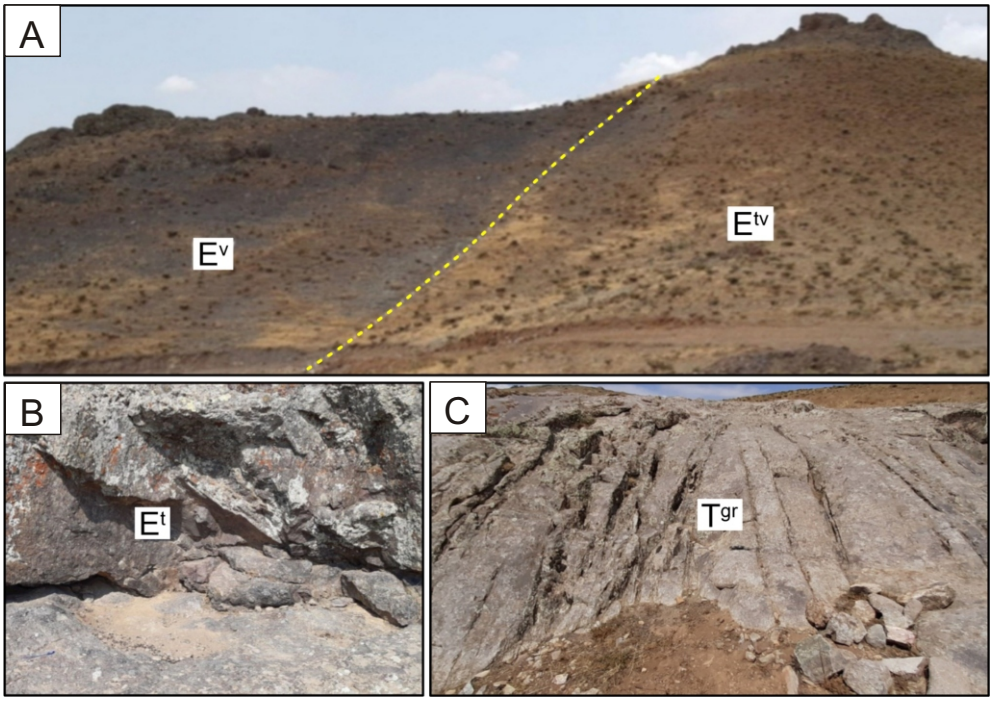

Fig. 3. Field photos of the lithological units in the Gh-Ku area

A – exposures of the lithological sequence of tuff, sandy tuff, andesite (E^{tv}), and andesite-basalt (E^v) (view towards the north); **B** – exposures of pyroclastic and tuff breccia units (E^t); **C** – exposure of a granite

of ±0.2°C). For determining the source of the ore-bearing fluid and its H_2S component, isotopic analyses of oxygen and sulphur were performed in laboratories at Arak University using an IRMS (Isotope Ratio Mass Spectrometer) system. The precisions of the measurements for sulphur and oxygen were ±0.1 and ±0.2‰, respectively.

ALTERATION

Field evidence and petrographic investigations show that the hydrothermal alteration at Gh-Ku is not pervasive, being mainly restricted to the wall rock margins of the veins and veinlets and the mineralized zones. The hydrothermal alteration in the study area includes four distinct types:

- silicic,
- phyllic,
- intermediate argillic,
- propylitic.

The first three are intimately affiliated with ore-bearing zones in the host rocks. The silicic zones are observed primarily in the margins of the ore-bearing quartz veins and veinlets, and outwards they gradually change to the sericitic zone. The silicic zones in the area are significant because of being associated with the ores (Fig. 4A), and because their high resistance to weathering means that they have high topographic relief at out-

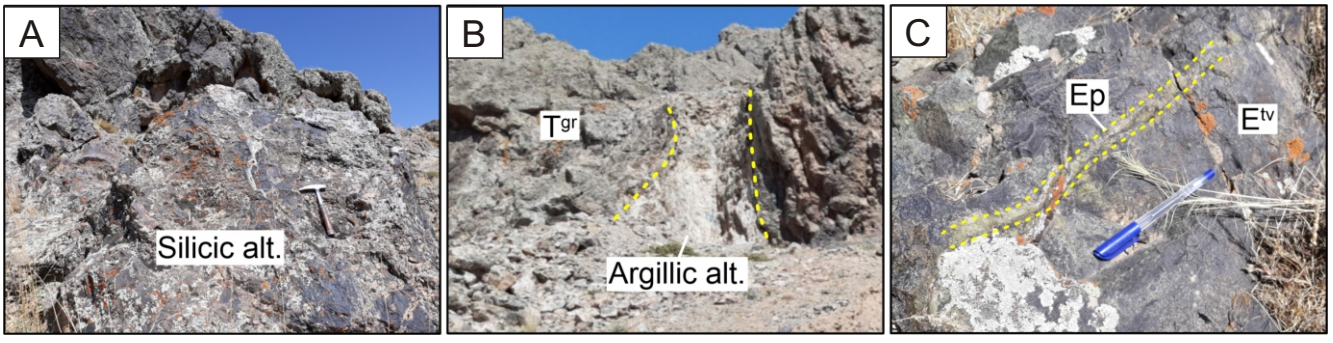

Fig. 4. Field photos depicting the surface expressions of the hydrothermal alteration zones at Gh-Ku

A – surface view of a silicic alteration zone; **B** – exposure of an intermediate argillic alteration zone; **C** – veinlets of epidote in a propylitic alteration zone; all abbreviations are from Whitney and Evans (2010); Ep – epidote; for other explanations see Figure 3

crop relative to the surrounding rocks. Quartz is the major mineral present in the silicic zone, accompanied by small amounts of adularia (Fig. 5A), which commonly occurs replacing primary silicate minerals in the host rocks. The phyllic alteration is limited in extent, is commonly observed around silicic zones, and is characterized by the presence of sericite, quartz, pyrite, and small amounts of clay minerals (Fig. 5B). In this alteration zone, sericite is mainly present replacing plagioclase. This zone gradually and outwards turns into the intermediate argillic alteration zone which appears as a white to yellow halo with relatively wider extent surrounding the ore-bearing veins (Fig. 4B). In places, this alteration is orange to red owing to the presence of Fe-oxides and hydroxides. This alteration zone is marked by clay minerals which commonly replace feldspar and sericite (Fig. 5C). The propylitic alteration zone has a relatively limited extent in the study area, being observed farther away from the ore-bearing veins. This alteration is recognized by its green colour at exposure and has affected most of the Eocene units (Fig. 4C). It formed by replacement of plagioclase, amphibole and biotite by epidote, chlorite and calcite (Fig. 5D-F).

MINERALIZATION

CHARACTERISTICS OF THE ORE-BEARING VEINS

Field observations show that mineralization at Gh-Ku took place as quartz veins and veinlets, mostly along the strike of fault and fracture zones. These veins and veinlets are hosted by the Eocene volcanic-pyroclastic and Oligocene intrusive (granite) units (Fig. 6A, B). Most of the quartz veins have NE–SW trends but some strike NW-SE with varying dips ranging from 70–90 . These veins have varying widths and lengths, ranging from 0.5 to 15 m and from 10 to 700 m, respectively, being milky white to dark grey in colour and red to brown in the weathered parts (due to Fe-oxides and hydroxides) or green (from the presence of malachite) (Fig. 6C). These veins and veinlets occasionally exhibit stockwork structure (Fig. 6D). The quartz crystals within them generally demonstrate massive, brecciated (Fig. 6E), comb (Fig. 6F), crustiform, and vug infill (Fig. 6G) textures. Mineralization within the quartz veins and veinlets consists of pyrite, chalcopyrite, galena, sphalerite, native gold, and Mn-oxides and hydroxides. These ore minerals occur as disseminated grains within the veins. The overall assays of Cu, Pb, Zn, Au and Ag in samples collected from the ore-bearing veins are 0.1, 0.4 and 0.35%; 0.2 and 10 ppm, respectively (TSIG, 2022).

MINERALIZATION STAGES

On the basis of the types of minerals and textural relationships in the ore-bearing veins and veinlets, the mineralization processes at Gh-Ku can be categorized into three distinct stages. During stage 1, minerals such as quartz, pyrite and chalcopyrite along with slight amounts of gold were deposited (Fig. 7A). In the course of the stage 2, quartz, galena, sphalerite and gold along with pyrite and chalcopyrite were precipitated (Fig. 7B). The sulphides of stages 1 and 2 occur as fine to coarse crystals within quartz veinlets. The quartz formed in stages 1 and 2 comprises fine to coarse crystals of milky white to grey colour. Stage 3 of mineralization is characterized by the presence of Mn-oxides and hydroxides (pyrolusite and psilomelane) together with quartz (Fig. 7C). The quartz crystals of this stage are also fine to coarse, displaying milky white to violet (amethystine) colour (Fig. 7D). From field observations and mesoscopic and microscopic investigations at Gh-Ku, the para-

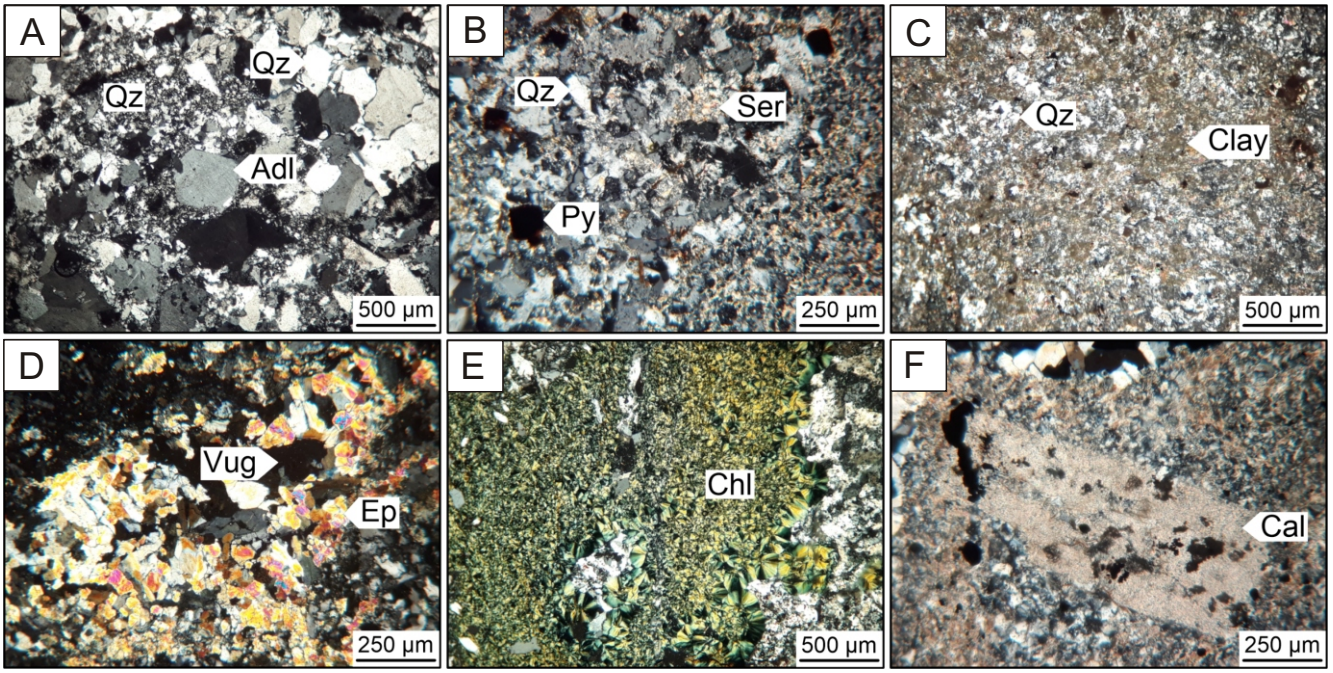

Fig. 5. Photomicrographs (xpl) of samples from the hydrothermal alteration zones at Gh-Ku

A – quartz and adularia in the silicic zone; **B** – sericite, quartz, and pyrite in the phyllic zone; **C** – the intermediate alteration zone in which the plagioclase has been replaced by clay minerals; **D** – the presence of euhedral epidote in the form of void-filling in the propylitic zone; **E** – formation of chlorite with spheroidal texture in the propylitic zone; **F** – replacement of plagioclase by calcite in the propylitic zone; Adl – adularia, Cal – calcite, Chl – chlorite, Clay – clay minerals, Ep – epidote, Py – pyrite, Qz – quartz, Ser – sericite

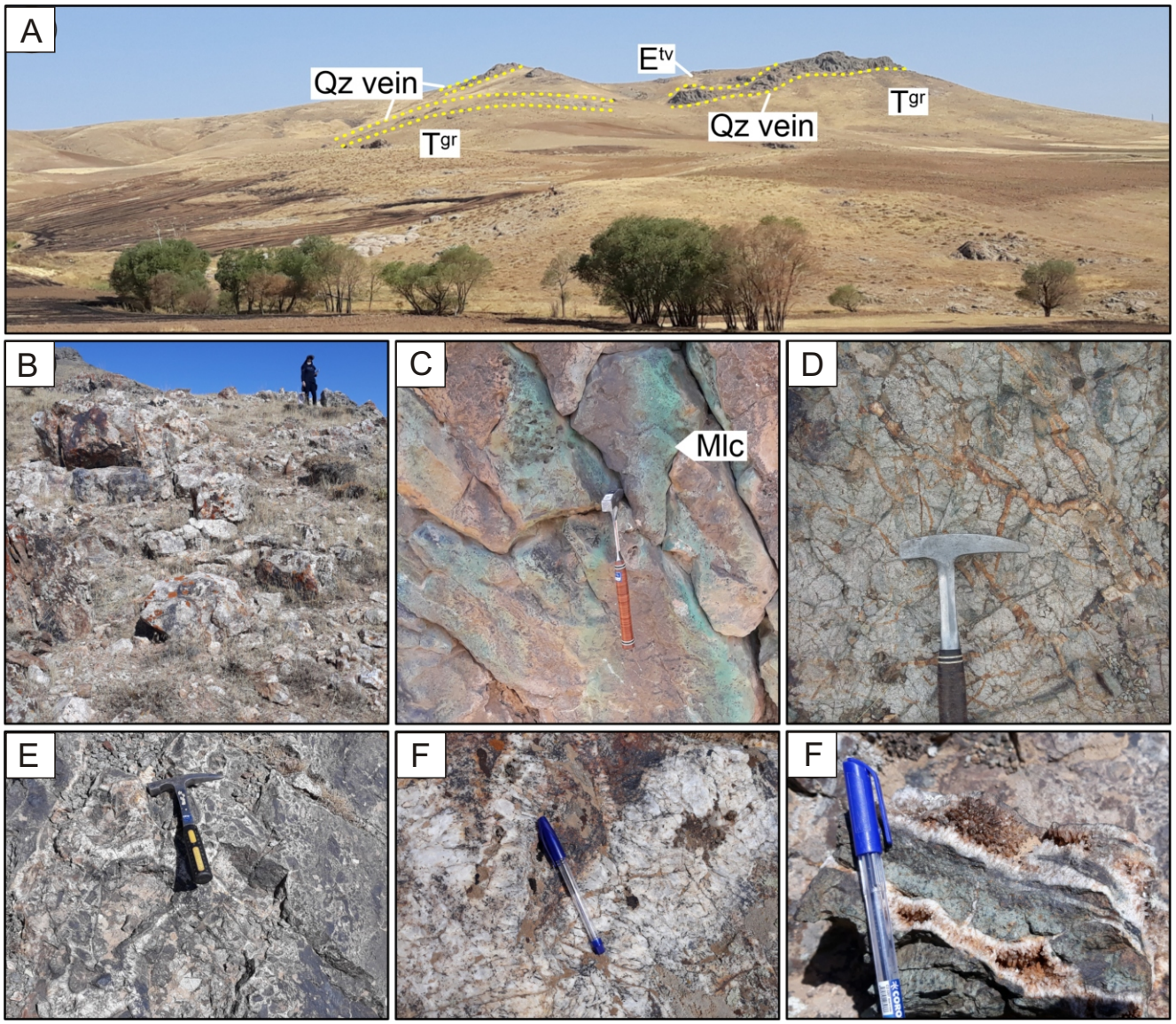

Fig. 6. Field photos of quartz veins and veinlets at Gh-Ku

A – exposures of quartz veins hosted by lithological units such as tuff, sandy tuff, andesite (E^{tv}), and granite (T^{gr}) (view towards the north-west); **B** – exposure of quartz veins in a granite (view towards the north-east); **C** – quartz vein containing malachite; **D** – stockwork structure in the quartz veins and veinlets; **E** – brecciation in the quartz veins and veinlets; **F** – quartz crystals with comb texture within quartz veins and veinlets; **G** – quartz crystals showing crustiform and open-space filling textures within quartz veins and veinlets; Mlc – malachite, Qz – quartz

genetic sequence of coexisting minerals (ore and gangue) and their relative abundance formed during hypogene and supergene processes is summarised in Figure 8.

TYPES OF ORE AND GANGUE MINERALS

The important ore minerals in the mineralized zones at Gh-Ku are pyrite, chalcopyrite, galena, sphalerite and gold accompanied by pyrolusite and psilomelane. Quartz, adularia, sericite, epidote, chlorite and calcite are the significant gangue minerals accompanying the ores. During the supergene processes, minerals such as cerussite, goethite, hematite, jarosite, bornite, covellite, chalcocite, digenite, cuprite, malachite and azurite formed. The ore and gangue minerals at Gh-Ku show, in general, various types of textures including vein and veinlet, massive, brecciated, disseminated, replacement, relict, cauliflower, comb, crustiform, cockade, vug infill, plumose, flamboyant and saccharoidal.

Pyrite occurs as very fine- to medium-grained (10 μm to 2 mm), anhedral to euhedral disseminated crystals within the quartz matrix (Figs. 9A and 10A). It is often replaced marginally and along the micro-fractures by secondary minerals: goethite, hematite, and jarosite exhibiting relict texture (Fig. 9A). In the hypogene zone, it is occasionally replaced by chalcopyrite indicating its earlier paragenetic deposition (Figs. 9B and 10B). Intergrowth of pyrite with chalcopyrite, however, is also common (Fig. 9C). Tiny inclusions of pyrite within galena and sphalerite were also observed. Chalcopyrite is the most abundant sulphide at Gh-Ku and occurs as fine- to medium-grained

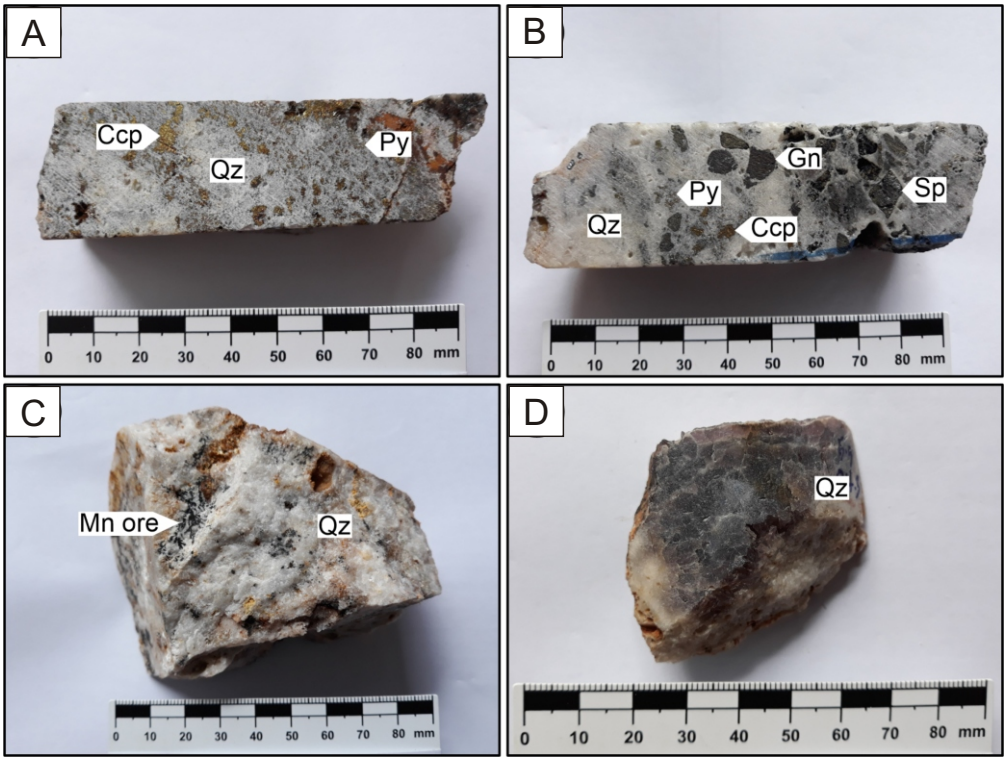

Fig. 7. Mesoscopic photos representing the different stages of mineralization at Gh-Ku

A – stage 1 of mineralization manifested by the presence of pyrite and chalcopyrite along with quartz; **B** – the presence of pyrite, chalcopyrite, galena and sphalerite together with quartz developed in stage 2 of the mineralization; **C** – formation of quartz and Mn-oxides and hydroxides during stage 3 of the mineralization; **D** – formation of quartz crystals of violet (amethystine) colour during stage 3 of the mineralization; Ccp – chalcopyrite, Gn – galena, Mn ore – manganese ore minerals, Py – pyrite, Qz – quartz, Sp – sphalerite

(up to 3 mm), anhedral to subhedral disseminated crystals within the silicic matrix (Fig. 10C). In the supergene zones, it was also marginally and along micro-fractures altered to goethite, bornite, covellite, chalcocite, digenite, cuprite, malachite, and azurite (Fig. 9B, D, E). In places where the supergene alteration is intense, it was almost entirely replaced by supergene minerals and shows relict texture. It typically shows intergrowths with pyrite, galena and sphalerite (Fig. 9C and F), but occasionally was replaced by galena and sphalerite so that inclusions of chalcopyrite within these minerals were also observed (Fig. 9C and G).

Galena mostly occurs as fine to medium-grained (up to 3 mm), anhedral to euhedral crystals in the silicic zones (Figs. 9G and 10D). It was concurrently precipitated with pyrite, chalcopyrite and sphalerite (Fig. 9C and G), and was replaced at its margins by cerussite in the supergene zone (Fig. 9H). Sphalerite occurs as medium- to coarse-grained (up to 2 cm), subhedral to euhedral crystals and is scattered within the silicic matrix (Figs. 9F and 10E). It shows intergrowth texture with pyrite, chalcopyrite and galena (Fig. 9C, F, G). In places, sphalerite along with galena replace and engulf pyrite and chalcopyrite crystals (Figs. 9G and 10A) suggesting that they formed after pyrite and chalcopyrite. The native gold is present as very fine-grained inclusions within quartz (Fig. 9I), pyrite, goethite and chalcopyrite (Figs. 9J and 10B, F). Pyrolusite occurs as fine- to medium-grained, anhedral to subhedral disseminated crystals within quartz veins and veinlets, and is more abundant than psilomelane (Fig. 9K). Psilomelane is accompanied by and coexisted with pyrolusite within quartz veins and veinlets and occasionally shows cauliflower texture (Fig. 9L).

Quartz is the most abundant gangue mineral at Gh-Ku and occurs as fine- to coarse-grained (<10 μm up to 5 cm), anhedral to euhedral crystals (Fig. 5A). It is commonly milky white, grey, and violet (amethystine) in colour but is occasionally colourless and transparent. The quartz crystals display typical veinlet, comb (Fig. 11A), crustiform (Fig. 11B), cockade (Fig. 11C), vug infill, plumose (Fig. 11D), flamboyant (Fig. 11E) and saccharoidal (Fig. 11F) textures. Adularia usually occurs as medium to coarse grains along with quartz crystals within the quartz veinlets (see Fig. 5A). Sericite is mainly present as fine flakes (see Fig. 5B). Epidote is observed as anhedral to euhedral crystals and displays veinlet, disseminated and vug infill textures (Fig. 5D). Chlorite primarily occurs as fine to medium flakes and shows veinlet, vug infill, and spheroidal textures (see Fig. 5E). Calcite is mostly present in the form of fine to medium crystals (Fig. 5F), and occasionally shows micro-veinlet textures.

FLUID INCLUSION (FI) STUDIES

The main objectives of the fluid inclusion studies were determinations of certain physico-chemical conditions (temperatures and salinities) of the hydrothermal ore-bearing solutions. Micro-thermometric studies have proven important in acquiring such information and contribute to better constraints on the evolution of hydrothermal fluids, and on ore genesis (Wilkinson, 2001; Van den Kerkhof and Hein, 2001; Bodnar et al., 2014). Considerations of the ore-containing veins and veinlets along with petrographic examinations of the ore and gangue minerals

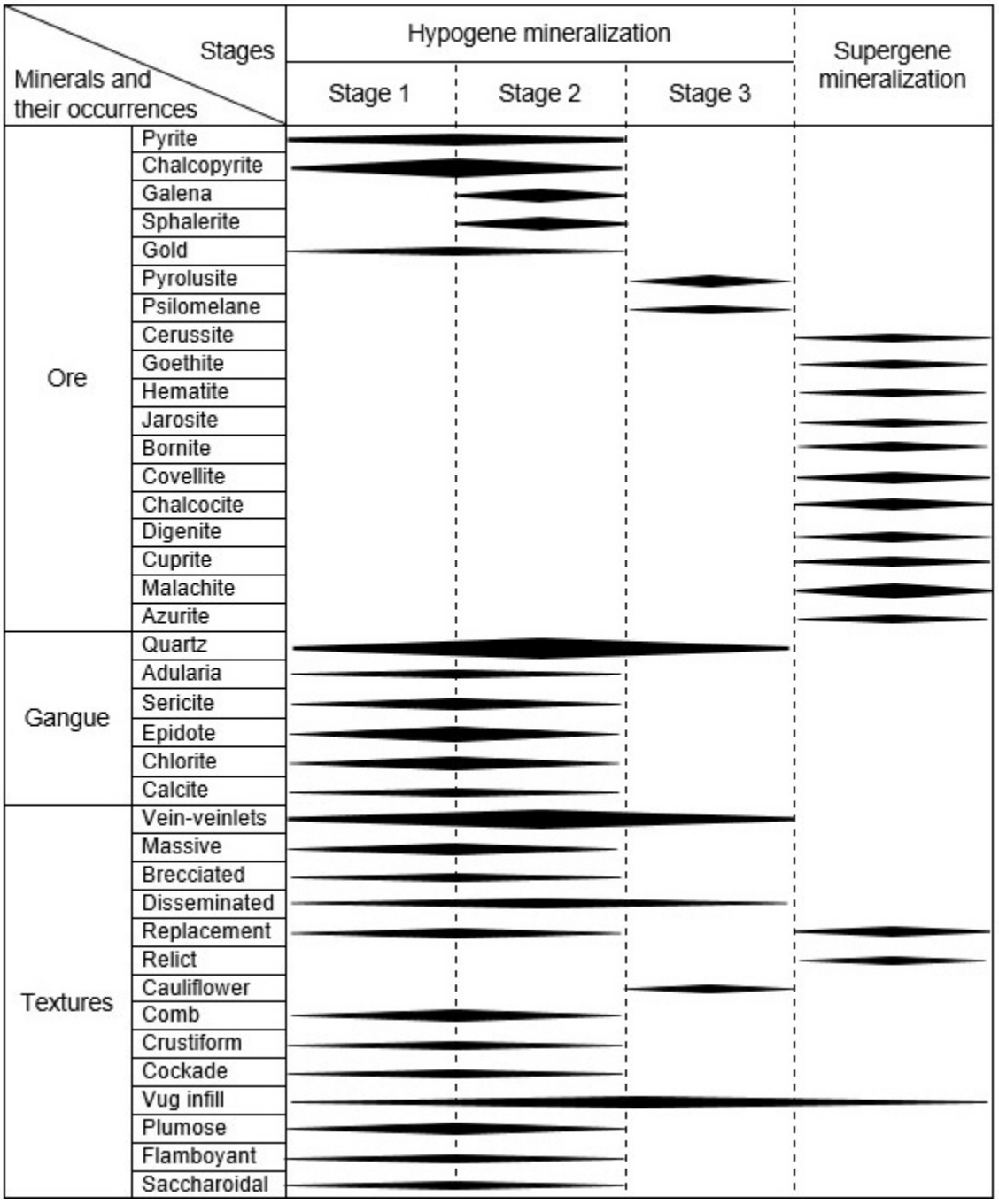

Fig. 8. Paragenetic sequence of the ore and gangue minerals and their relative abundance along with various types of textures they show at Gh-Ku

at Gh-Ku delineated that the quartz crystals within the quartz veins and veinlets, through being cogenetic with the sulphides, are very suitable for micro-thermometric analysis.

During examinations by optical microscopy, certain physical characteristics of the FIs including their shape, type, size, degree of fill and phase ratio were recognized. The FIs studied at Gh-Ku had irregular, triangle, square, polygonal, acicular, ellipsoidal, vermicular, elongated, spheroidal and negative quartz crystal shapes (Fig. 12). According to criteria suggested by Roedder (1984) and Goldstein (2003), three types of FI (primary and secondary) were distinguished in samples from the study area (Fig. 12). The micro-thermometric measurements were done exclusively on the primary FIs. The FIs vary in size from <10 to 100 μm but most of them have sizes within the range of 10 to 50 m. A necking-down phenomenon was also recognized in few cases (Fig. 12C). On the basis of the ratios of the phase content and also according to Shepherd et al. (1985), the FIs were classified into three types: (1) liquid-rich 2-phase (LV) inclusions, (2) mono-phase vapour (V) inclusions, and (3) vapour-rich 2-phase (VL) inclusions (Fig. 12). There was no evidence to indicate the presence of liquid CO_2 and/or solid daughter phases. The liquid-rich 2-phase (LV) inclusions are relatively more abundant than the other types, and their liquid phase is dominant and occupies >70 vol.% of the FI. The vapour phase

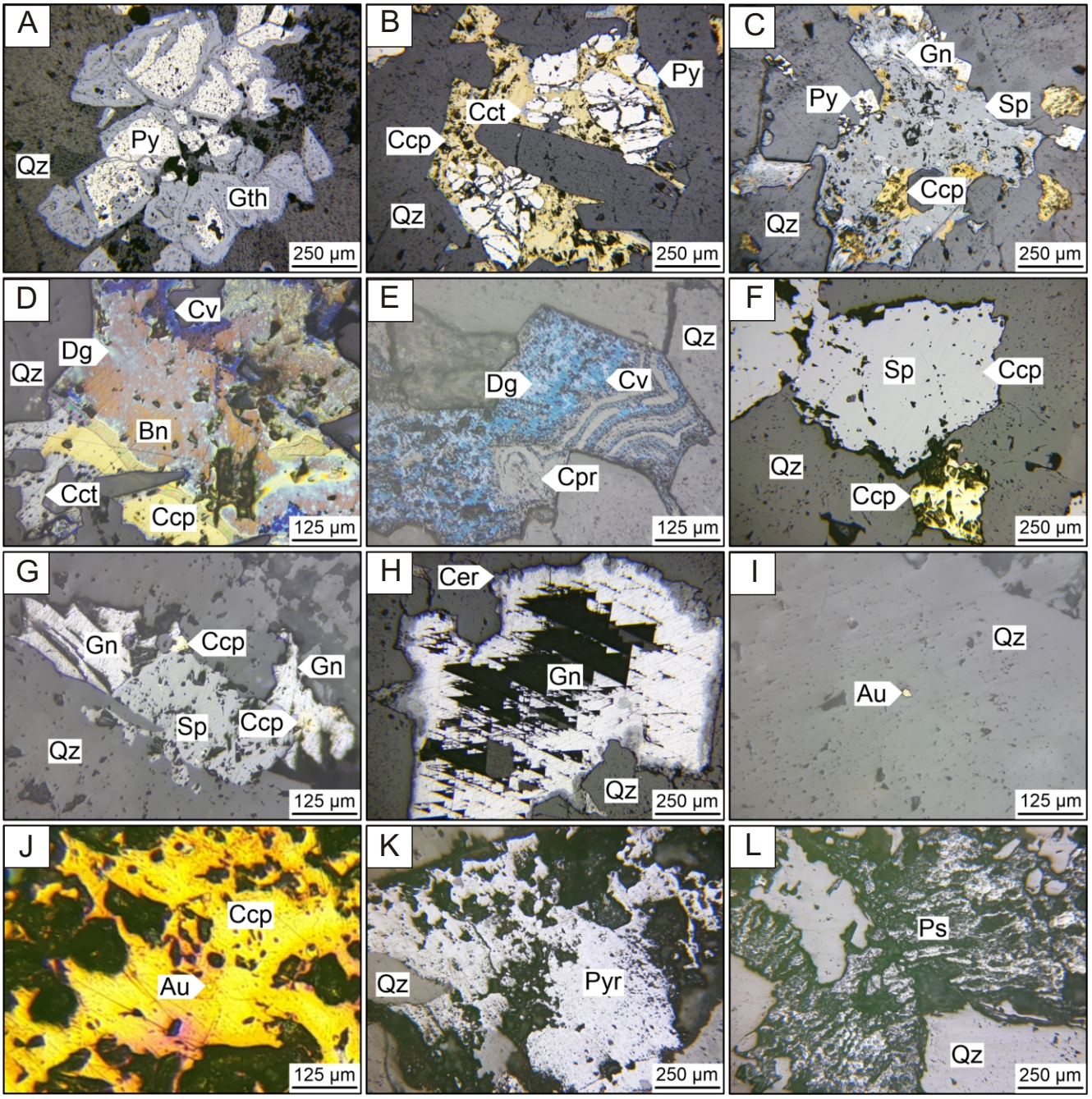

Fig. 9. Photomicrographs (ppl) of the ore and gangue minerals within quartz veins and veinlets at Gh-Ku

A – pyrite crystals replaced by goethite; **B** – pyrite crystals replaced and rimmed by chalcopyrite; replacement of chalcopyrite by chalcocite is visible; **C** – intergrowth of pyrite, chalcopyrite, galena and sphalerite; replacement of chalcopyrite by galena and sphalerite is visible; **D** – replacement of chalcopyrite by bornite, covellite, chalcocite and digenite; **E** – complete replacement of primary Cu minerals by covellite, digenite and cuprite; **F** – intergrowth of chalcopyrite and sphalerite; **G** – intergrowth of galena and sphalerite; the presence of inclusions of chalcopyrite within sphalerite and galena in this picture is also noticeable; **H** – presence of coarse galena crystal displaying typical galena pits with replacement by cerussite; **I** – presence of native gold within quartz matrix; **J** – presence of gold inclusions within chalcopyrite; **K** – coarse crystal of pyrolusite; **L** – psilomelane with cauliflower texture; Au – gold, Bn – bornite, Ccp – chalcopyrite, Cct – chalcocite, Cer – cerussite, Cpr – cuprite, Cv – covellite, Dg – digenite, Gn – galena, Gth – goethite, Ps – psilomelane, Py – pyrite, Pyr – pyrolusite, Qz – quartz, Sp – sphalerite

in the vapour-rich 2-phase (VL) inclusions occupies almost >80 vol.% of the FI. In most samples studied, all of the three types coexisted and present next to each other (Fig. 12L), that could be indicative of boiling.

Micro-thermometric analyses of the selected samples were carried out on 90 liquid-rich 2-phase FIs. Because it was not feasible to detect the liquid phase in the vapour-rich 2-phase (VL) FIs during the heating process and there was a possibility

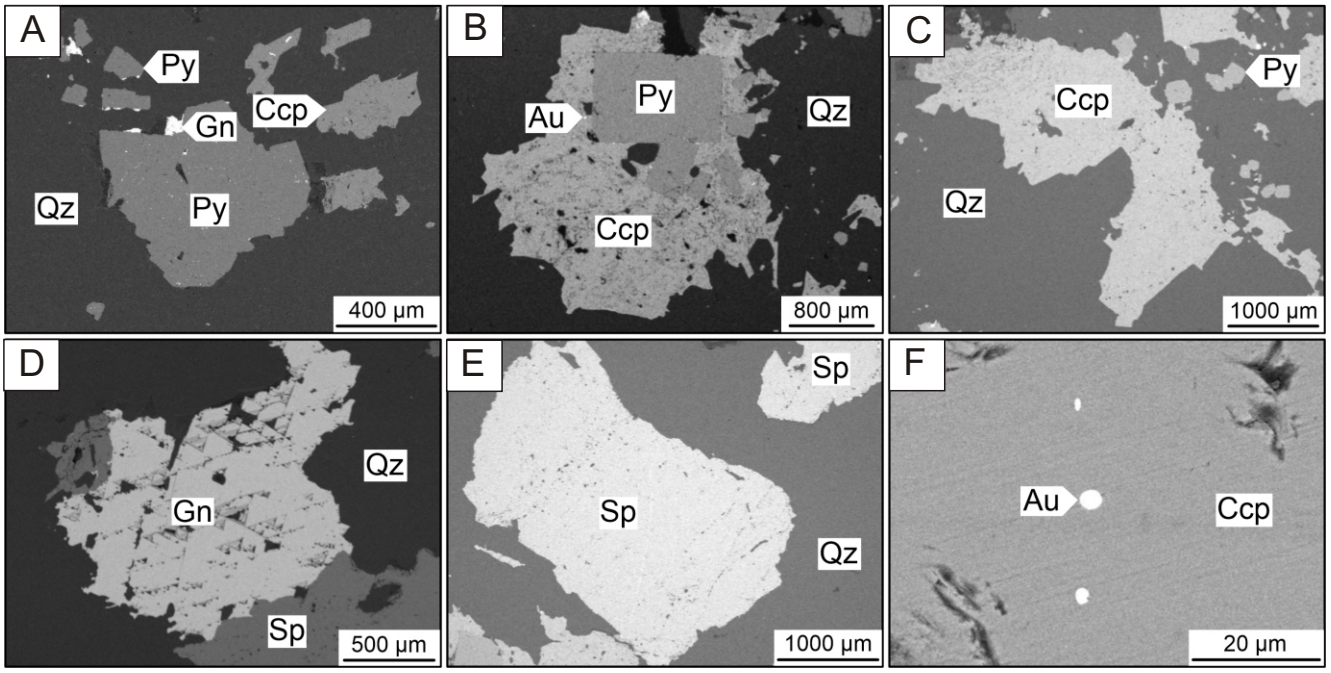

Fig. 10. Backscattered electron (BSE) images of the ore and gangue minerals in quartz veins and veinlets at Gh-Ku

A – fine and coarse crystals of pyrite in association with chalcopyrite; replacement of pyrite by galena is visible; **B** – overgrowth of pyrite by chalcopyrite with small gold inclusions within chalcopyrite; **C** – coarse crystal of chalcopyrite next to pyrite; **D** – coarse crystals of galena and sphalerite; **E** – coarse crystal of sphalerite; **F** – blebs of gold within chalcopyrite; Au – gold, Ccp – chalcopyrite, Gn – galena, Py – pyrite, Qz – quartz, Sp – sphalerite

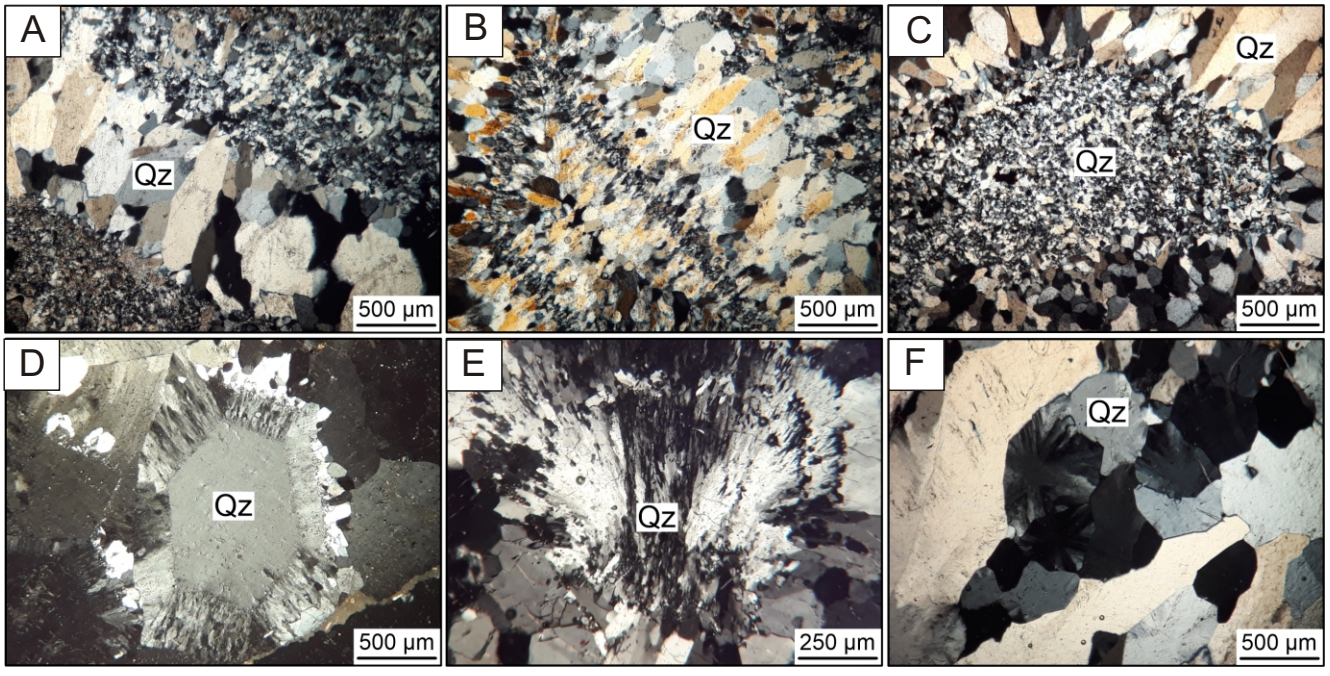

Fig. 11. Photomicrographs (xpl) of quartz crystals depicting various types of texture at Gh-Ku

A – quartz with comb texture; **B** – crustiform texture displayed by quartz crystals; **C** – cockade texture in quartz crystals; **D** – quartz with plumose texture; **E** – flamboyant texture exhibited by quartz crystals; **F** – quartz grains with saccharoidal texture; Qz – quartz

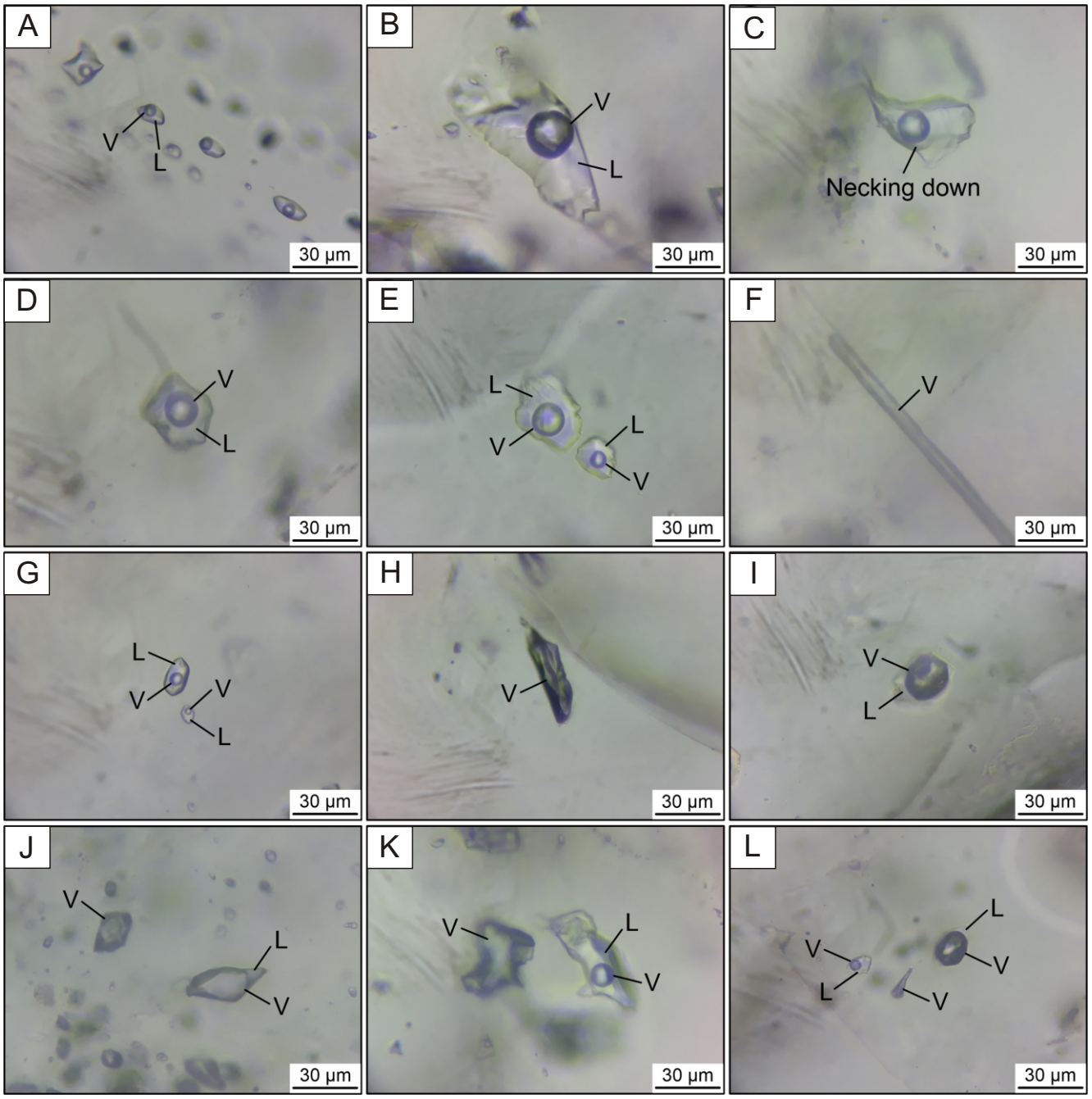

Fig. 12. Photomicrographs (ppl) of various types of FI in quartz crystals at Gh-Ku (A – secondary FI and B–L – primary FI)

A – liquid-rich 2-phase (LV) FI of regular shape; **B** – liquid-rich 2-phase (LV) FI of triangular shape; **C** – necking-down in liquid-rich 2-phase FI; **D** – liquid-rich 2-phase (LV) polygonal FI; **E** – liquid-rich 2-phase (LV) elliptical FI; **F** – mono-phase vapour (V) acicular FI; **G** – liquid-rich 2-phase (LV) FI with negative quartz crystal shape; **H** – mono-phase vapour (V) FI; **I** – vapour-rich 2-phase (VL) FI; **J** – coexistence of vapour-rich 2-phase (VL) FI with mono-phase vapour (V) FI; **K** – coexistence of liquid-rich 2-phase (LV) FI with mono-phase vapour (V) FI; **L** – coexistence of 2-phase (LV and VL) FI with mono-phase vapour (V) FI

of error, these FIs were not selected for micro-thermometric analysis. During the cooling procedure, the salinities and types of solutes were determined by measuring the eutectic (first melting) point and the last melting point of ice (Roedder, 1984; Davis et al., 1990; Goldstein and Reynolds, 1994; Goldstein, 2003; Prokofiev et al., 2010). The eutectic points of the first melting (T_{fm}) of the samples of stages 1, 2, and 3 of mineralization vary from –19 to –26°C, from –21 to –24°C, and from –18 to –23°C, respectively (see Table 1), which generally correspond essentially with a H_2O-NaCl system which may also have small amounts of KCl. Therefore, it can be envisaged that NaCl is the dominant salt in the FIs studied. The last melting points (Tm_{ice}) of the FIs within the quartz crystals of stages 1 and 2 of the mineralization range from –3.8 to –6.9°C and from –2.5 to –4.9°C, respectively (see Table 1 and Fig.13A). The Tm_{ice} values in FIs of stage 3 of the mineralization range from –1.5 to –3.3°C (see

Table 1

Summary of the micro-thermometric data obtained from liquid-rich 2-phase (LV) FIs in quartz crystals within ore-bearing quartz veins and veinlets at Gh-Ku

Mineral	Incl. type	T_{fm} [°C]	Tm_{ice} [°C]	Th range [°C]	Salinity [wt.% NaCl equiv.]	ρ [g/cm3]
Stage 1 Qz (n = 30)	LV	–19 to –26	–3.8 to –6.9	275–325	6.2–10.4	0.71–0.88
Stage 2 Qz (n = 30)	LV	–21 to –24	–2.5 to –4.9	253–312	4.2–7.7	0.78–0.90
Stage 3 Qz (n = 30)	LV	–18 to –23	–1.5 to –3.3	215–284	2.6–5.4	0.76–0.91

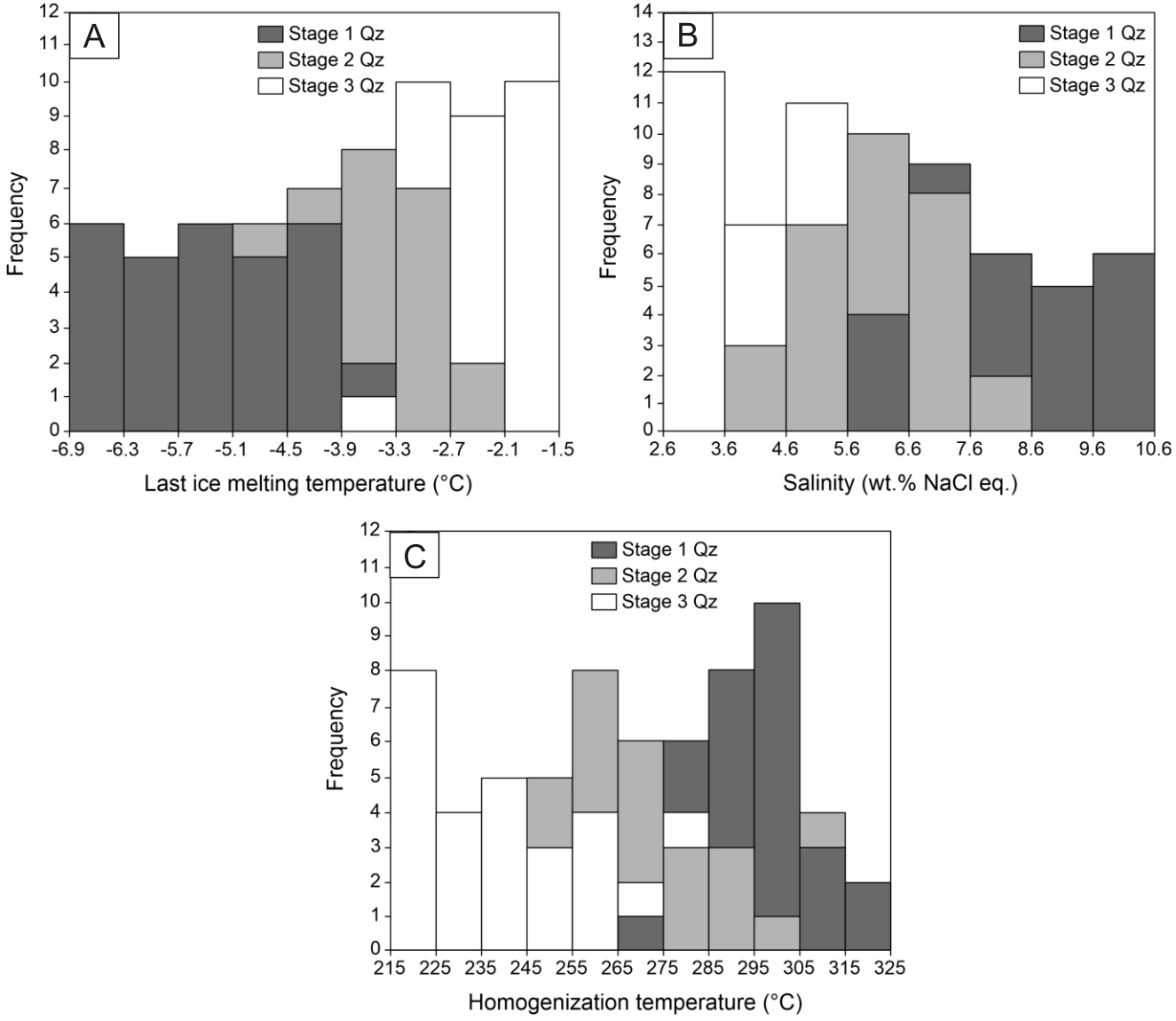

Fig. 13. Diagrams of frequency distribution of A – the last melting points of ice, B – salinity, and C – homogenization temperature (Th) for liquid-rich 2-phase FIs in the quartz crystals at Gh-Ku

Table 1 and Fig. 13A). On the basis of the Tm_{ice} values and also referring to the table of Bodnar (2003), the FI salinity values of stages 1, 2, and 3 of the mineralization were determined to be within the range of 6.2 to 10.4 wt.%, 4.2 to 7.7 wt.%, and 2.6 to 5.4 wt.% NaCl eq., respectively (see Table 1 and Fig. 13B). During heating, all the liquid-rich 2-phase FIs homogenized into a liquid state. The homogenization temperatures (Th) of FIs in stages 1, 2, and 3 of the quartz crystals demonstrated a range of 275 to 325°C, 253 to 312°C, and 215 to 284°C, respectively (see Table 1 and Fig. 13C). The overall range of densities of the FIs is 0.71 to 0.91 g/cm^3 (see Table 1 and Fig. 14A).

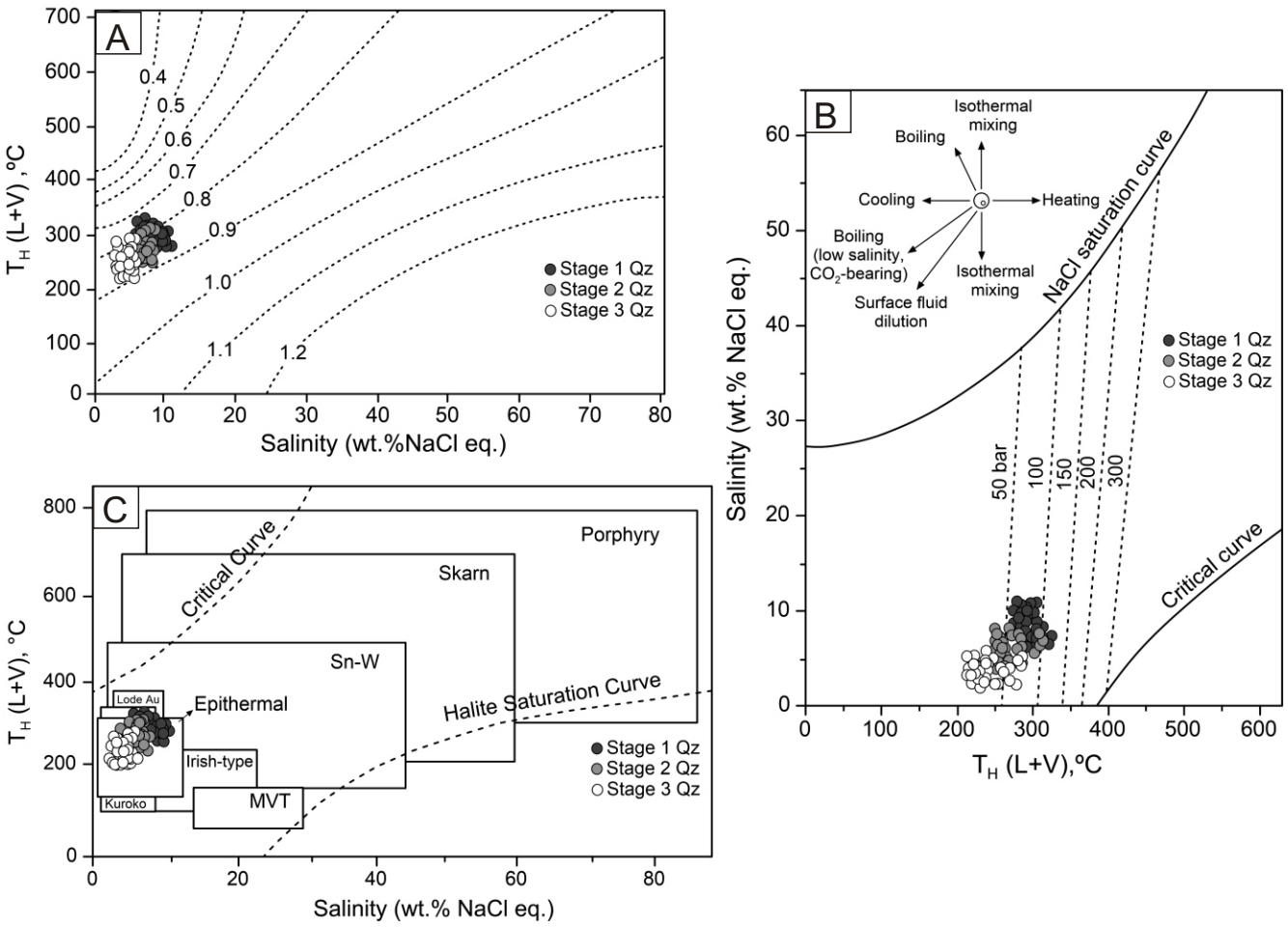

Fig. 14A – variation of density values in FIs on a bivariate plot of Th vs salinity (Wilkinson, 2001); B – bivariate diagram of Th vs salinity (Shepherd et al., 1985; Wilkinson, 2001) on which the FI data points delineate both boiling and mixing evolutionary trends; NaCl saturation and critical curves are from Ahmad and Rose (1980) and the dashed lines related to vapour pressure are from Roedder (1984); C – bivariate diagram of Th vs salinity (Wilkinson, 2001) on which the FI from Gh-Ku plot principally within the epithermal domain

STABLE ISOTOPE STUDIES

Studies of stable isotopes in ore deposits are important, because they furnish useful information on the source of hydrothermal fluids, origin of ore-forming components, mineralization temperatures, and genesis of the deposit (Ohmoto and Rye, 1979; Faure et al., 2002; Hoefs, 2015). To obtain such information, four sulphide samples (chalcopyrite, galena and sphalerite) for sulphur isotopes and four cogenetic quartz samples for oxygen isotopes were selected from quartz veins and veinlets at Gh-Ku. The isotopic data obtained for oxygen and sulphur are listed in Table 2. According to the data obtained, the measured $\delta^{18}O$ values for stages 1, 2, and 3 of the quartz are +18.2, +18.8, and +18‰, respectively. The oxygen isotopic compositions of the hydrothermal fluids in equilibrium with quartz were calculated by taking the average temperature of homogenization (Th) of the FIs studied and also applying the equation of Méheut et al. (2007). The calculated $\delta^{18}O$ values of the hydrothermal fluids for stages 1, 2, and 3 of the mineralization are +12.5, +12.1, and +9.7‰, respectively (see Table 2). The $\delta^{34}S$ values of the sulphide minerals (chalcopyrite, galena and sphalerite) vary from –1.6 to –3.6‰ (see Table 2). By taking the average Th value of the FIs studied as the equilibrium temperature and using the equation of Li and Liu (2006), the $\delta^{34}S$ values of the ore-bearing fluids in equilibrium with the sulphides range from –1.5 to –3.4‰ (see Table 2).

DISCUSSION

EVIDENCE FOR BOILING

Coexistence of FIs of LV and VL types within the host crystals may provide evidence for boiling of the ore-forming fluids (White and Hedenquist, 1995; Ronacher et al., 2000; Prokofiev et al., 2010; Moncada et al., 2017). The presence of V type FIs may also indicate boiling (Albinson et al., 2001; Moncada et al., 2017). The coexistence and simultaneous trapping of LV, VL, and V FI types within quartz crystals at Gh-Ku (Fig. 12L) strongly suggests their entrapment from boiling fluids. However, sometimes these types of FI may co-exist as a result of necking-down or leakage (Ramboz et al., 1982; Rusk et al., 2008).

The presence of adularia may also indicate boiling of the ore-forming fluids (Simmons and Browne, 2000; Moncada et al., 2012). The existence of adularia within quartz veins and veinlets at Gh-Ku (see Fig. 5A) may be proof of boiling. Expul-

Table 2

List of compositional values of stable isotopes of oxygen ($\delta^{18}O$) and sulphur ($\delta^{34}S$) in samples from the study area

Sample no.	Stages of mineralization	Mineral	$\delta^{18}O_{quartz}$ [‰ VSMOW]	$\delta^{18}O_{H2O}$ [‰VSMOW]	$\delta^{34}S_{sulphide}$ [‰ CDT]	$\delta^{34}S_{H2S}$ [‰ CDT]
T-01	1	chalcopyrite			–3.3	–3.4
T-02	2	chalcopyrite			–2.4	–2.5
T-03	2	galena			–3.6	–1.5
T-04	2	sphalerite			–1.6	–1.9
T-05	1	quartz	+18.2	+12.5		
T-06	2	quartz	+18.8	+12.1		
T-07	2	quartz	+18.2	+11.5		
T-08	3	quartz	+18.0	+9.7		

sion of CO_2 during boiling causes pH increase of the solution and consequently results in the stability of adularia (Browne, 1978; André-Mayer et al., 2002). The precipitation of quartz crystals with crustiform (see Figs. 6G and 11B), cockade (see Fig. 11C) and plumose (see Fig. 11D) textures in the study area suggest boiling. Crustiform and cockade textures in quartz veins and veinlets may point to rapid precipitation of quartz crystals in relatively shallow epithermal systems (Roedder, 1984; Fournier, 1985; Bodnar et al., 1985). These textures usually develop during rapid opening of fractures in connection to pressure decrease and the ensuing temperature decrease associated with boiling (Thiersch et al., 1997; Taylor, 2009; Moncada et al., 2012). The plumose texture displayed by quartz crystals might have formed as a result of boiling which in turn brought about silica saturation, rapid temperature decrease, and subsequent precipitation of amorphous silica (Henley and Hughes, 2000).

The evidence of boiling at Gh-Ku can be further demonstrated by the development of hydrothermal breccias and ore-bearing brecciated veins (see Fig. 6E) which are normally caused by sudden pressure drop (from lithostatic to hydrostatic). In general, such evidence in the study area can individually denote boiling events in the hydrothermal system (Cole and Drummond, 1986; Jobson et al., 1994; Çiçek and Oyman, 2016). Moreover, the veins and veinlets in the study area have sharp contacts with the host rocks, which strongly suggest that they were formed via filling of open spaces under hydrostatic pressure (Hedenquist et al., 1998; Liu et al., 2014; Ouyang et al., 2014) which in turn caused the development of hydrothermal breccias (Thiersch et al., 1997; Muntean and Einaudi, 2001).

SOURCE(S) OF ORE-BEARING FLUIDS

The $\delta^{18}O$ values of the hydrothermal fluids in equilibrium with quartz at Gh-Ku vary from +9.7 to +12.5‰ (see Table 2) indicating that the ore-bearing solutions had a predominantly magmatic signature but in the course of mineralization became progressively cooled and diluted. Fluids of stage 3 of the mineralization, relative to the earlier stages (1 and 2), were depleted in $\delta^{18}O$ (see Table 2) which may denote the involvement of meteoric waters in the hydrothermal system (Rye, 1993; Simmons et al., 2005; Li et al., 2018b; Yu et al., 2018; Yuan et al., 2019). The salinity data suggest that the ore-forming fluids from the early to the late stages of mineralization were dilute. These results are in agreement with the isotopic evidence. The salinities obtained from the FI analyses (see Table 1) illustrate that the ore-forming fluids were initially derived from magmatic sources and became diluted by meteoric waters during the next stages of mineralization. Similar processes have been reported for many magmatic-hydrothermal systems from other parts of the world (Thiersch et al., 1997; Camprubí and Albinson, 2007; Zhai et al., 2013; Xie et al., 2017) and particularly from NW Iran (Zamanian et al., 2019; Kouhestani et al., 2019a, b, 2020; Ferdowsi et al., 2021; Ghasemi Siani et al., 2022).

The $\delta^{34}S$ values of the sulphides (see Table 2) reflect that they were developed under stable physico-chemical conditions and that the sulphur was derived from a relatively homogeneous magmatic source (Faure, 1986; Calagari, 2003; Chen et al., 2009; Hoefs, 2015). In general, the measured $\delta^{18}O$ and $\delta^{34}S$ values suggest that the hydrothermal fluids at Gh-Ku had chiefly magmatic components.

EVOLUTIONARY TREND OF THE ORE-FORMING FLUIDS

The micro-thermometric data at Gh-Ku show that the ore-bearing fluids belong predominantly to a H_2O-NaCl system of intermediate temperature and low salinity. The temperatures of this system decreased gradually from 325 to 215°C during the three stages of mineralization. According to Figure 14B, boiling and mixing of hypogene magmatic fluids with low-temperature and low-salinity solutions (probably of meteoric origin) were the two crucial mechanisms causing the precipitation of the base and precious metals in the Gh-Ku area. The micro-thermometric data on the bivariate diagram of salinity versus homogenization temperature (Th) (Fig. 14C) plot in the domain of epithermal fluids, so close to the domain of magmatic fluids (Roedder, 1984). Salinities of magmatic fluids commonly vary from <5 to 10 wt.% NaCl eq. (Burnham, 1979; Hedenquist and Lowenstern, 1994; Yardley, 2005; Simmons and Brown, 2006), although magmatic fluids with higher salinities have also been reported (Yardley and Bodnar, 2014). Therefore, the relatively wide range of salinity values at Gh-Ku can be indicative of mixing of the magmatic fluids with underground waters of meteoric origin. These results are in agreement with the oxygen isotope data. Boiling causes salinity increase in the liquid phase (Wilkinson, 2001; Calagari, 2004; Canet et al., 2011) and has

been widely reported for epithermal systems (Simmons and Browne, 2000; Simpson et al., 2001; Camprubí and Albinson, 2007; Klemm et al., 2007).

TRAPPING PRESSURE AND DEPTH OF MINERALIZATION

Considering the evidence of boiling at Gh-Ku, there is no need for the measured homogenization temperatures (Th) of the FI to be corrected for pressure (Simeone and Simmons, 1999). In such conditions, the homogenization temperatures can be regarded as trapping temperatures and the trapping pressures of the ore-bearing fluids can be equal to hydrostatic pressures at homogenization temperatures (Roedder and Bodnar, 1980; Ouyang et al., 2014). By following Albinson (1988) and Hedenquist et al. (1998), the highest Th (284 to 325°C) were taken for determining the pressure and depth of mineralization at Gh-Ku. The trapping pressures of the FIs were determined to be within the range of 70 to 120 bars (Fig. 14B), approximately equal to hydrostatic depths of 700 to 1200 m below the water table. Similar depths have also been widely inferred for epithermal deposits from other parts of the world (Cooke and Simmons, 2000; Simmons et al., 2005; Pirajno, 2009).

MINERALIZATION TYPE

With due attention to the evidence reported here and also by the many other workers (White and Hedenquist, 1990; Hedenquist et al., 2000; Sillitoe and Hedenquist, 2003; Einaudi et al., 2003; Moritz et al., 2003; Simmons et al., 2005; Pirajno, 2009; Moncada et al., 2012, 2017; Leary et al., 2016; Moussa et al., 2019), the mineralization at Gh-Ku can be classified as an epithermal base and precious metals deposit. This inference can be justified as follows:

- the mineralization at Gh-Ku was structurally controlled by faults and hosted by volcanic-pyroclastic units and a granite intrusive body;
- the hydrothermal alterations are characterized by mineral assemblages such as adularia, sericite, epidote, chlorite and calcite;
- the ore minerals are pyrite, chalcopyrite, galena, sphalerite, pyrolusite and psilomelane which are accompanied by the gangue mineral assemblage of quartz, adularia, sericite, epidote, chlorite and calcite;
- the ore and gangue minerals represent epithermal structures and textures including vein/veinlet, brecciated, cauliflower, comb, crustification, cockade, vug infill, plumose, flamboyant and saccharoidal.

Additionally, the relatively lower temperature, salinity and density of the ore-forming fluids at Gh-Ku are characteristics of epithermal base and precious metal deposits which have also been reported for similar deposits from different areas of NW Iran (Heidari et al., 2015; Mehrabi et al., 2016; Zamanian et al., 2019; Kouhestani et al., 2019a, b, 2020; Miranvari et al., 2020; Ferdowsi et al., 2021; Ebrahimi et al., 2021; Ghasemi Siani et al., 2022) as well as from other parts of the world (Albinson et al., 2001; Sabeva et al., 2017; Li et al., 2018a, b; Soberano et al., 2021; Chen et al., 2022). Furthermore, the depth of mineralization at Gh-Ku was determined to be within the range of 700 to 1200 m, analogous to those of most other epithermal base and precious metal deposits (Hedenquist et al., 2000; Cooke and Simmons, 2000; Simmons et al., 2005). The presence of adularia and carbonates and lack of vuggy quartz and advanced argillic alteration (with a mineral assemblage of alunite, kaolinite and pyrophyllite) and also lack of a mineral assemblage such as alunite, enargite, luzonite and tetrahedrite in the ore-bearing veins and veinlets show that the mineralization at Gh-Ku is neither of high-sulphidation (HS) nor intermediate-sulphidation (IS) style (Hedenquist et al., 2000). Generally, the geological characteristics, paragenetic sequence, ore and gangue textures, types of alteration, and nature of ore-forming fluids at Gh-Ku provide convincing evidence that the mineralization here has the greatest resemblance to epithermal deposits of low-sulphidation (LS) style.

CONCLUSIONS

1. Hydrothermal solutions in the Gh-Ku area caused the formation of quartz veins and veinlets along structural (fault) zones. The volcanic-pyroclastic rocks together with granite are the host rocks for the ore-bearing quartz veins and veinlets.

2. Silicic, phyllic, intermediate argillic and propylitic alteration zones were developed around the quartz veins and veinlets.

3. The mineralization in the study area took place in three distinct stages. The mineral assemblages formed during stage 1 are quartz, pyrite, chalcopyrite and gold; during stage 2 quartz, pyrite, chalcopyrite, galena, sphalerite and gold; and during stage 3 quartz and Mn-oxides and hydroxides (pyrolusite and psilomelane).

4. The micro-thermometric considerations of liquid-rich 2-phase fluid inclusions in the quartz crystals showed that homogenization temperatures (Th) and salinities of the inclusions studied vary within the range of 215 to 325°C and 2.6 to 10.4 wt.% NaCl eq., respectively.

5. On the basis of micro-thermometric data, the ore-forming fluids at Gh-Ku had densities within the range of 0.71 to 0.91 g/cm^3 and experienced hydrostatic pressures varying from 70 to 120 bars, corresponding to depths of mineralization approximately ranging from 700 to 1200 m below the water table.

6. The isotopic values of oxygen ($\delta^{18}O_{H2O}$: from +9.7 to +12.5‰) and sulphur ($\delta^{34}S_{H2S}$: from –1.5 to –3.4‰) indicate that the ore-forming fluids at Gh-Ku had a predominantly magmatic signature and gradually mixed with meteoric solutions during the evolutionary trend of mineralization. Moreover, consideration of micro-thermometric and stable isotope data indicate that boiling and mixing were two effective factors contributing to the deposition of the base and precious metals in the study area.

7. The geological characteristics, mineralization, ore and gangue textures, types of hydrothermal alteration, and nature of the ore-forming fluids, signify that mineralization at Gh-Ku is essentially of epithermal type with a low-sulphidation (LS) style.

Acknowledgements. This research is a part of the first author's Ph.D. thesis project which was mainly funded by the Bureau of Research Deputy and Complementary Education of the University of Tabriz. The authors would like to thank the authorities of this Bureau. We also appreciate the generous cooperation of the authorities at the Tavangaran Sahand Industrial Company for permitting us to have access to their diamond drill cores in the study area. Our grateful appreciation is extended to two anonymous reviewers for their suggestions and critical comments on this paper.

REFERENCES

Ahmad, S.N., Rose, A.W., 1980. Fluid inclusions in porphyry and skarn ore at Santa Rita, New Mexico. Economic Geology, **75**: 229–250. https://doi.org/10.2113/gsecongeo.75.2.229

Albinson, T.F., 1988. Geologic reconstruction of paleosurfaces in the Sombrerete, Colorado, and Fresnillo districts, Zacatecas State, Mexico. Economic Geology, **83**: 1647–1667. https://doi.org/10.2113/gsecongeo.83.8.1647

Albinson, T., Norman, D.I., Cole, D., Chomiak, B., 2001. Controls on formation of low-sulfidation epithermal deposits in Mexico: Constraints from fluid inclusion and stable isotope data. In: New Mines and Discoveries in Mexico and Central America (eds. T. Albinson and C.E. Nelson): 1–32. Society of Economic Geologists, Littleton. https://doi.org/10.5382/SP.08.01

André-Mayer, A.S., Leroy, J.L., Bailly, L., Chauvet, A., Marcoux, E., Grancea, L., Liosa, F., Rosas, J., 2002. Boiling and vertical mineralization zoning: a case study from the Apacheta low-sulfidation epithermal gold-silver deposit, southern Peru. Mineralium Deposita, **37**: 452–464. https://doi.org/10.1007/s00126-001-0247-2

Behrouzi, A., Amini Fazl, A., Amini Azar, R., 1997. Geological map of Bostanabad, scale 1:100000. Geological Survey of Iran.

Bodnar, R.J., 2003. Introduction to aqueous-electrolyte fluid inclusions. In: Fluid Inclusions: Analysis and Interpretation (eds. I. Samson, A. Anderson and D. Marshal): 81–100. Mineralogical Association of Canada, Vancouver.

Bodnar, R.J., Burnham, C.W., Sterner, S.M., 1985. Synthetic fluid inclusions in natural quartz. III. Determination of phase equilibrium properties in the system H_2O-NaCl to 1000°C and 1500 bars. Geochimica et Cosmochimica Acta, **49**: 1861–1873. https://doi.org/10.1016/0016-7037(85)90081-X

Bodnar, R.J., Lecumberri-Sanchez, P., Moncada, D., Steele-MacInnis, M., 2014. Fluid inclusions in hydrothermal ore deposits. In: Treatise on Geochemistry: 119–142. Elevier. https://doi.org/10.1016/B978-0-08-095975-7.01105-0

Browne, P.R.L., 1978. Hydrothermal alteration in active geothermal fields. Annual Review of Earth and Planetary Sciences, **6**: 229–248. https://doi.org/10.1146/annurev.ea.06.050178.001305

Burnham, C.W., 1979. Magmas and hydrothermal fluids. In: Geochemistry of Hydrothermal Ore Deposits (ed. H.L. Barnes): 71–136. John Wiley and Sons, New York.

Calagari, A.A., 2003. Stable isotope (S, O, H and C) studies of phyllic and potassic-phyllic alteration zones of the porphyry copper deposit at Sungun, East Azarbaijan, Iran. Journal of Asian Earth Sciences, **21**: 767–780. https://doi.org/10.1016/S1367-9120(02)00083-4

Calagari, A.A., 2004. Fluid inclusion studies in quartz veinlets in the porphyry copper deposit at Sungun, East Azarbaidjan, Iran. Journal of Asian Earth Sciences, **23**: 179–189. https://doi.org/10.1016/S1367-9120(03)00085-3

Camprubí, A., Albinson, T., 2007. Epithermal deposits in Mexico: Update of current knowledge, and an empirical reclassification. GSA Special Papers, **422:** 377–415. https://doi.org/10.1130/2007.2422(14)

Canet, C., Franco, S.I., Prol-Ledesma, R.M., González-Partida, E., Villanueva-Estrada, R.E., 2011. A model of boiling for fluid inclusion studies: application to the Bolaños Ag-Au-Pb-Zn epithermal deposit, Western Mexico. Journal of Geochemical Exploration, **110**: 118–125> https://doi.org/10.1016/j.gexplo.2011.04.005

Chen, Y.J., Pirajno, F., Li, N., Guo, D.S., Lai, Y., 2009. Isotope systematics and fluid inclusion studies of the Qiyugou breccia pipe-hosted gold deposit, Qinling Orogen, Henan province, China: implications for ore genesis. Ore Geology Reviews, **35**: 245–261; https://doi.org/10.1016/j.oregeorev.2008.11.003

Chen, C., Wu, T., Sha, D., Li, D., Yang, Z., Zhang, J., Shang, Q., 2022. Genesis of the Dongpuzi Gold Deposit in the Liaodong Peninsula, NE China: Constraints from geology, fluid inclusion, and C-H-O-S-Pb isotopes. Minerals, **12**: 1008. https://doi.org/10.3390/min12081008

Çiçek, M., Oyman, T., 2016. Origin and evolution of hydrothermal fluids in epithermal Pb-Zn-Cu±Au±Ag deposits at Koru and Tesbihdere mining districts, Çanakkale, Biga Peninsula. NW Turkey. Ore Geology Reviews, **78**: 176–195. https://doi.org/10.1016/j.oregeorev.2016.03.020

Cole, D.R., Drummond, S.E., 1986. The effect of transport and boiling on Ag/Au ratios in hydrothermal solutions: a preliminary assessment and possible implications for the formation of epithermal precious-metal ore deposits. Journal of Geochemical Exploration, **25**: 45–79. https://doi.org/10.1016/0375-6742(86)90007-5

Cooke, D.R., Simmons, S.F., 2000. Characteristics and genesis of epithermal gold deposits. Reviews in Economic Geology, **13**: 221–244. https://doi.org/10.5382/Rev.13.06

Davis, D.W., Lowenstein, T.K., Spencer, R.J., 1990. Melting behavior of fluid inclusions in laboratory-grown halite crystals in the systems NaCl-H_2O, NaCl-KCl-H_2O, NaCl-$MgCl_2$-H_2O, and NaCl-$CaCl_2$-H_2O. Geochimica et Cosmochimica Acta, **54**: 591–601. https://doi.org/10.1016/0016-7037(90)90355-O

Ebrahimi, S., Pan, Y., Rezaeian, M., 2021. Origin and evolution of the Masjed Daghi Cu-Au-Mo porphyry and gold epithermal vein system, NW Iran: constraints from fluid inclusions and sulfur isotope studies. Mineralogy and Petrology, **115**: 643–662.~ https://doi.org/10.1007/s00710-021-00761-z

Einaudi, M.T., Hedenquist, J.W., Inan, E.E., 2003. Sulfidation state of fluids in active and extinct hydrothermal systems: transitions from porphyry to epithermal environments. In: Volcanic, geothermal, and ore-forming fluids: rulers and witnesses of processes within the earth (eds. S.F. Simmons and I. Graham): 285–313. Society of Economic Geologists, Littleton. https://doi.org/10.5382/SP.10.15

Faure, G., 1986. Principles of Isotope Geology. John Wiley and Sons, New York.

Faure, K., Matsuhisa, Y., Metsugi, H., Mizota, C., Hayashi, S., 2002. The Hishikari Au-Ag epithermal deposit, Japan: Oxygen and hydrogen isotope evidence in determining the source of paleohydrothermal fluids. Economic Geology, **97**: 481–498. https://doi.org/10.2113/gsecongeo.97.3.481

Ferdowsi, R., Calagari, A.A., Simmonds, V., Miranvari, A., 2021. Evolution of the gold (copper) mineralization in the porphyry stock and the related skarn zones and epithermal veins in the Astarghan area, NW Iran: evidence from fluid inclusion, mineral chemistry and sulfur isotope analyses. Ore Geology Reviews, **136**: 104196. https://doi.org/10.1016/j.oregeorev.2021.104196

Fournier, R.O., 1985. The behavior of silica in hydrothermal solutions. In: Geology and Geochemistry of Epithermal Systems (eds. B.R. Berger and P.M. Bethke): 45–61. Society of Economic Geologists, Littleton. https://doi.org/10.5382/Rev.02.03

Ghasemi Siani, M., Mehrabi, B., Nazarian, M., Lotfi, M., Corfu, F., 2022. Geology and genesis of the Chomalu polymetallic deposit, NW Iran. Ore Geology Reviews, **143**: 104763. https://doi.org/10.1016/j.oregeorev.2022.104763

Goldstein, R.H., 2003. Petrographic analysis of fluid inclusions. In: Fluid Inclusions: Analysis and Interpretation (eds. I. Samson, A. Anderson and D. Marshall): 9–53. Mineral Associated of Canada, Vancouver.

Goldstein, R.H., Reynolds, T.J., 1994. Systematics of fluid inclusions in diagenetic minerals. SEPM Short Course, **31**. https://doi.org/10.2110/scn.94.31

Hassani Soughi, Z., Calagari, A.A., Sohrabi, Gh., 2021. Gold-sulfide mineralization and microthermometry in quartz veins and veinlets in the Gharehchay area, south of Tikmehdash, East-Azarbaidjan province (in Persian). Iranian journal of Crystallography and Mineralogy, **29**: 97–110. doi:10.52547/ijcm.29.1.97

Hedenquist, J.W., Lowenstern, J.B., 1994. The role of magmas in the formation of hydrothermal ore deposits. Nature, **370**: 519–527. https://doi.org/10.1038/370519a0

Hedenquist, J.W., Arribas, A., Reynolds, T.J., 1998. Evolution of an intrusion-centered hydrothermal system: far southeast Lepanto porphyry and epithermal Cu-Au deposits, Philippines. Economic Geology, **93**: 373–404. https://doi.org/10.2113/gsecongeo.93.4.373

Hedenquist, J.W., Arribas, A.R., Gonzalez-Urien, E., 2000. Exploration for epithermal gold deposits. In: Gold in 2000 (eds. S.G. Hagemann and P.E. Brown): 245–277. Society of Economic Geologists, Littleton. https://doi.org/10.5382/Rev.13.07

Heidari, S.M., Daliran, F., Paquette, J.L., Gasquet, D., 2015. Geology, timing, and genesis of the high sulfidation Au (-Cu) deposit of Touzlar, NW Iran. Ore Geology Reviews, **65**: 460–486. https://doi.org/10.1016/j.oregeorev.2014.05.013

Henley, R.W., Hughes, G.O., 2000. Underground fumaroles: "Excess heat" effects in vein formation. Economic Geology, **95**: 453–466. https://doi.org/10.2113/gsecongeo.95.3.453

Hoefs, J., 2015. Stable Isotope Geochemistry, 7th edition. Springer International Publishing, Switzerland.

Jobson, D.H., Boulter, C.A., Foster, R.P., 1994. Structural controls and genesis of epithermal gold-bearing breccias at the Lebong Tandai mine, Western Sumatra. Indonesia. Journal of Geochemical Exploration, **50**: 409–428. https://doi.org/10.1016/0375-6742(94)90034-5

Klemm, L.M., Pettke, T., Heinrich, C.A., Campos, E., 2007. Hydrothermal evolution of the El Teniente deposit, Chile: Porphyry Cu-Mo ore deposition from low-salinity magmatic fluids. Economic Geology, **102**: 1021–1045. https://doi.org/10.2113/gsecongeo.102.6.1021

Kouhestani, H., Mokhtari, M.A.A., Qin, K.Z., Zhao, J.X., 2019a. Fluid inclusion and stable isotope constraints on ore Genesis of the Zajkan epithermal base metal deposit, Tarom-Hashtjin metallogenic belt, NW Iran. Ore Geology Reviews, **109**: 564–584. https://doi.org/10.1016/j.oregeorev.2019.05.014

Kouhestani, H., Mokhtari, M.A.A., Qin, K.Z., Zhao, J.X., 2019b. Origin and evolution of hydrothermal fluids in the Marshoun epithermal Pb-Zn-Cu (Ag) deposit, Tarom-Hashtjin metallogenic belt, NW Iran. Ore Geology Reviews, **113**: 103087. https://doi.org/10.1016/j.oregeorev.2019.103087

Kouhestani, H., Mokhtari, M.A.A., Qin, K.Z., Zhang, X.N., 2020. Genesis of the Abbasabad epithermal base metal deposit, NW Iran: evidences from ore geology, fluid inclusion and O-S isotopes. Ore Geology Reviews, **126**: 103752. https://doi.org/10.1016/j.oregeorev.2020.103752

Leary, S., Sillitoe, R.H., Stewart, P.W., Roa, K.J., Nicolson, B.E., 2016. Discovery, geology, and origin of the Fruta del Norte epithermal gold-silver deposit, southeastern Ecuador. Economic Geology, **111**: 1043–1072. https://doi.org/10.2113/econgeo.111.5.1043

Li, S.N., Ni, P., Bao, T., Li, C.Z., Xiang, H.L., Wang, G.G., Huang, B., Chi, Z., Dai, B.Z., Ding, J.Y., 2018a. Geology, fluid inclusion, and stable isotope systematics of the Dongyang epithermal gold deposit, Fujian Province, southeast China: implications for ore genesis and mineral exploration. Journal of Geochemical Exploration, **195**: 16–30. https://doi.org/10.1016/j.gexplo.2018.02.009

Li, S.N., Ni, P., Bao, T., Xiang, H.L., Chi, Z., Wang, G.G., Bao, H., Ding, J.Y., Dai, B.Z., 2018b. Genesis of the Ancun epithermal gold deposit, southeast China: Evidence from fluid inclusion and stable isotope data. Journal of Geochemical Exploration, **195**: 157–177. https://doi.org/10.1016/j.gexplo.2018.01.016

Li, Y.B., Liu, J.M., 2006. Calculation of sulfur isotope fractionation in sulfides. Geochimica et Cosmochimica Acta, **70**: 1789–1795. https://doi.org/10.1016/j.gca.2005.12.015

Liu, J., Mao, J.W., Wu, G., Wang, F., Luo, D.F., Hu, Y.Q., Li, T.G., 2014. Fluid inclusions and H-O–S–Pb isotope systematics of the Chalukou giant porphyry Mo deposit, Heilongjiang Province. China. Ore Geology Reviews, **59**: 83–96. https://doi.org/10.1016/j.oregeorev.2013.12.006

Maghsoudi, A., Rahmani, M., Rashidi, B., 2005. Gold deposits and indications of Iran (in Persian). Arian Zamin Publication, Tehran.

Méheut, M., Lazzeri, M., Balan, E., Mauri, F., 2007. Equilibrium isotopic fractionation in the kaolinite, quartz, water system: prediction from first-principles density-functional theory. Geochimica et Cosmochimica Acta, **71**: 3170–3181. https://doi.org/10.1016/j.gca.2007.04.012

Mehrabi, B., Ghasemi Siani, M., Goldfarb, R., Azizi, H., Ganerod, M., Marsh, E.E., 2016. Mineral assemblages, fluid evolution and genesis of polymetallic epithermal veins, Gulojeh district, NW Iran. Ore Geology Reviews, **78**: 41–57. https://doi.org/10.1016/j.oregeorev.2016.03.016

Miranvari, A.S.A., Calagari, A.A., Ferdowsi, R., 2020. Evolution of ore-forming fluids in the Sarilar gold-bearing silicic veins: evidence from fluid inclusions and sulphur stable isotopes studies, East-Azarbaidjan, NW of Iran. Periodic di Mineralogia, **89**: 265–278. https://rosa.uniroma1.it/rosa04/periodico_di_mineralogia/article/view/16745/16122

Moncada, D., Mutchler, S., Nieto, A., Reynolds, T.J., Rimstidt, J.D., Bodnar, R.J., 2012. Mineral textures and fluid inclusion petrography of the epithermal Ag-Au deposits at Guanajuato, Mexico: application to exploration. Journal of Geochemical Exploration, **114**: 20–35. https://doi.org/10.1016/j.gexplo.2011.12.001

Moncada, D., Baker, D., Bodnar, R.J., 2017. Mineralogical, petrographic and fluid inclusion evidence for the link between boiling and epithermal Ag-Au mineralization in the La Luz area, Guanajuato Mining District, Mexico. Ore Geology Reviews, **89**: 143–170. https://doi.org/10.1016/j.oregeorev.2017.05.024

Moritz, R., Jackquat, S., Chambefort, I., Fontignie, D., 2003. Controls on ore formation at high sulfidation Au–Cu Chelopech deposit, Bulgaria: Evidence from infrared fluid inclusion microthermometry of enargite and isotope systematics of barite. In: Mineral Exploration and Sustainable Development (ed. D.G. Eliopoulos): 1209–1212. Millpress, Rotterdam.

Moussa, N., Boiron, M.C., Grassineau, N.V., Asael, D., Fouquet, Y., Le Gall, B., Rolet, J., Etoubleau, J., Delacourt, C., 2019. Mineralogy, fluid inclusions and stable isotope study of epithermal Au-Ag-Bi-Te mineralization from the SE Afar Rift (Djibouti). Ore Geology Reviews, **111**: 102916. https://doi.org/10.1016/j.oregeorev.2019.05.002

Muntean, J.L., Einaudi, M.T., 2001. Porphyry-epithermal transition: Maricunga Belt, Northern Chile. Economic Geology, **96**: 743–772. https://doi.org/10.2113/gsecongeo.96.4.743

Nabavi, M., 1976. An Introduction to the Geology of Iran (in Persian). Geological Survey of Iran Publication, Tehran.

Ohmoto, H., Rye, R.O., 1979. Isotope of sulfur and carbon. In: Geochemistry of Hydrothermal Ore Deposits (ed. H.L. Barnes): 509–567. John Wiley and Sons, New York.

Ouyang, H., Wu, X., Mao, J.W., Su, H., Santosh, M., Zhou, Z., Li, C., 2014. The nature and timing of ore formation in the Budunhua copper deposit, southern Great Xing'an Range: evidence from geology, fluid inclusions, and U-Pb and Re-Os geochronology. Ore Geology Reviews, **63**: 238–251. https://doi.org/10.1016/j.oregeorev.2014.05.016

Pirajno, F., 2009. Hydrothermal Processes and Mineral Systems. Springer, Berlin.

Prokofiev, V.Y., Garofalo, P.S., Bortnikov, N.S., Kovalenker, V.A., Zorina, L.D., Grichuk, D.V., Selektor, S.L., 2010. Fluid inclusion constraints on the genesis of gold in the Darasun district (eastern Transbaikalia), Russia. Economic Geology, **105**: 395–416. https://doi.org/10.2113/gsecongeo.105.2.395

Ramboz, C., Pichavant, M., Weisbrod, A., 1982. Fluid immiscibility in natural processes: use and misuse of fluid inclusion data: II. Interpretation of fluid inclusion data in terms of immiscibility. Chemical Geology, **37**: 29–48. https://doi.org/10.1016/0009-2541(82)90065-1

Richards, J.P., Wilkinson, D., Ullrich, T., 2006. Geology of the Sari Gunay epithermal gold deposit, northwest Iran. Economic Geology, **101**: 1455–1496. https://doi.org/10.2113/gsecongeo.101.8.1455

Roedder, E., 1984. Fluid Inclusions. Reviews in Mineralogy, **12**.

Roedder, E., Bodnar, R.J., 1980. Geologic pressure determinations from fluid inclusion studies. Annual Review of Earth and Planetary Sciences, **8**: 263–301. https://doi.org/10.1146/annurev.ea.08.050180.001403

Ronacher, E., Richards, J.P., Johnston, M.D., 2000. Evidence for fluid phase separation in high-grade ore zones at the Porgera gold deposit, Papua New Guinea. Mineralium Deposita, **35**: 683–688. https://doi.org/10.1007/s001260050271

Rusk, B.G., Reed, M.H., Dilles, J.H., 2008. Fluid inclusion evidence for magmatic-hydrothermal fluid evolution in the porphyry copper-molybdenum deposit at Butte, Montana. Economic Geology, **103**: 307–334. https://doi.org/10.2113/gsecongeo.103.2.307

Rye, R.O., 1993. The evolution of magmatic fluids in the epithermal environment: the stable isotope perspective. Economic Geology, **88**: 733–753. https://doi.org/10.2113/gsecongeo.88.3.733

Sabeva, R., Mladenova, V., Mogessie, A., 2017. Ore petrology, hydrothermal alteration, fluid inclusions, and sulfur stable isotopes of the Milin Kamak intermediate sulfidation epithermal Au-Ag deposit in Western Srednogorie, Bulgaria. Ore Geology Reviews, **88**: 400–415. https://doi.org/10.1016/j.oregeorev.2017.05.013

Shepherd, T.J., Ranbin, A.H., Alderton, D.H.M., 1985. A Practical Guide to Fluid Inclusion Studies. Blackie, Glasgow.

Sillitoe, R.H., Hedenquist, J.W., 2003. Linkages between Volcanotectonic Settings, Ore-Fluid Compositions, and Epithermal Precious Metal deposits. In: Volcanic, Geothermal and Ore-forming Fluids: Rulers and Witnesses of Processes within the Earth (eds. S.F. Simmons and I.J. Graham): 315–343. Society of Economic Geologists Special Publication. https://doi.org/10.5382/SP.10.16

Simeone, R., Simmons, S.F., 1999. Mineralogical and fluid inclusion studies of low sulfidation epithermal veins at Osilo (Sardinia), Italy. Mineralium Deposita, **34**: 705–717. https://doi.org/10.1007/s001260050229

Simmons, S.F., Browne, P.R.L., 2000. Hydrothermal minerals and precious metals in the Broadlands-Ohaaki geothermal system: Implications for understanding low-sulfidation epithermal environments. Economic Geology, **95**: 971–999. https://doi.org/10.2113/gsecongeo.95.5.971

Simmons, S.F., Brown, K.L., 2006. Gold in magmatic hydrothermal solutions and the rapid formation of a giant ore deposit. Science, **314**: 288–291. doi:10.1126/science.1132866

Simmons, S.F., White, N.C., John, D.A., 2005. Geological characteristics of epithermal precious and base metal deposits. In: One Hundredth Anniversary Volume (eds. J.W. Hedenquist, J.F.H. Thompson, J.R. Goldfarb and J.P. Richards): 485–522. Society of Economic Geologists, Littleton. https://doi.org/10.5382/AV100.16

Simpson, M.P., Mauk, J.L., Simmons, S.F., 2001. Hydrothermal alteration and hydrologic evolution of the Golden Cross epithermal Au-Ag deposit, New Zealand. Economic Geology, **96**: 773–796.https://doi.org/10.2113/gsecongeo.96.4.773

Soberano, O.B., Gabo-Ratio, J.A.S., Queaño, K.L., Dimalanta, C.B., Yumul, Jr, G.P., Andal, E.S., Yonezu, K., Boyce, A.J., 2021. Mineral chemistry, fluid inclusion and stable isotope studies of the Suyoc epithermal veins: Insights to Au-Cu mineralization in southern Mankayan Mineral District, Philippines. Ore Geology Reviews, **131**: 104035. https://doi.org/10.1016/j.oregeorev.2021.104035

Taylor, R., 2009. Ore Textures: Recognition and Interpretation. Springer-Verlag, Berlin.

Thiersch, P.C., Williams-Jones, A.E., Clark, J.R., 1997. Epithermal mineralization and ore controls of the Shasta Au–Ag deposit, Toodoggone District, British Columbia, Canada. Mineralium Deposita, **32**: 44–57. https://doi.org/10.1007/s001260050071

TSIG., 2022. The report of the end of the exploration operation of Tikmehdash polymetal area (in Persian). Tavangaran Sahand Industrial Group, Iran, Report.

Van den Kerkhof, A.M., Hein, U.F., 2001. Fluid inclusion petrography. Lithos, **55**: 27–47. https://doi.org/10.1016/S0024-4937(00)00037-2

White, N.C., Hedenquist, J.W., 1990. Epithermal environments and styles of mineralization: variations and their causes, and guidelines for exploration. Journal of Geochemical Exploration, **36**: 445–474. https://doi.org/10.1016/0375-6742(90)90063-G

White, N.C., Hedenquist, J.W., 1995. Epithermal gold deposits: styles, characteristics and exploration. SEG Discovery, **I 27**: 1–13. https://doi.org/10.5382/SEGnews.1995-23.fea

Whitney, D.L., Evans, B.W., 2010. Abbreviations for names of rock-forming minerals. American Mineralogist, **95**: 185–187. https://doi.org/10.2138/am.2010.3371

Wilkinson, J.J., 2001. Fluid inclusions in hydrothermal ore deposits. Lithos, **55**: 229–272. https://doi.org/10.1016/S0024-4937(00)00047-5

Xie, Y., Li, L., Wang, B., Li, G., Liud, H., Li, Y., Dong, S., Zhou, J., 2017. Genesis of the Zhaxikang epithermal Pb-Zn-Sb deposit in southern Tibet, China: evidence for a magmatic link. Ore Geology Reviews, **80**: 891–909. https://doi.org/10.1016/j.oregeorev.2016.08.007

Yardley, B.W.D., 2005. Metal concentrations in crustal fluids and their relationship to ore formation. Economic Geology, **100**: 613–632. https://doi.org/10.2113/gsecongeo.100.4.613

Yardley, B.W.D., Bodnar, R.J., 2014. Fluids in the continental crust. Geochemical Perspectives, **3**: 1–127. https://10.7185/geochempersp.3.1

Yu, J., Li, N., Shu, S.P., Zhang, B., Guo, J.P., Chen, Y.J., 2018. Geology, fluid inclusion and H-O-S isotopes of the Kuruer Cu-Au deposit in Western Tianshan, Xinjiang, China. Ore Geology Reviews, **100**: 237–249. https://doi.org/10.1016/j.oregeorev.2017.07.016

Yuan, Z.Z., Li, Z.K., Zhao, X.F., Sun, H.S., Qiu, H.N., Li, J.W., 2019. New constraints on the genesis of the giant Dayingezhuang gold (silver) deposit in the Jiaodong district. North China Craton. Ore Geology Reviews, **112**: 103038. https://doi.org/10.1016/j.oregeorev.2019.103038

Zamanian, H., Rahmani, S., Zareisahameih, R., 2019. Fluid inclusion and stable isotope study of the Lubin-Zardeh epithermal Cu-Au deposit in Zanjan Province, NW Iran: implications for ore genesis. Ore Geology Reviews, **112**: 103014. https://doi.org/10.1016/j.oregeorev.2019.103014

Zhai, D.G., Liu, J.J., Wang, J.P., Yao, M.J., Wu, S.H., Fu, C., Liu, Z.J., Wang, S.G., Li, Y.X., 2013. Fluid evolution of the Jiawula Ag-Pb-Zn deposit, Inner Mongolia: mineralogical, fluid inclusion, and stable isotopic evidence. International Geology Review, **55**: 204–224. https://doi.org/10.1080/00206814.2012.692905